Article

Ligand-induced monoubiquitination of BIK1 regulates plant immunity

https://doi.org/10.1038/s41586-020-2210-3

Received: 12 September 2018

Accepted: 21 February 2020

Published online: 22 April 2020

Check for updates

Xiyu Ma[1,2], Lucas A. N. Claus[3,4], Michelle E. Leslie[5,10,11], Kai Tao[6,11], Zhiping Wu[7,8,11], Jun Liu[1,2], Xiao Yu[2,9], Bo Li[2,9], Jinggeng Zhou[1,2], Daniel V. Savatin[3,4], Junmin Peng[7,8], Brett M. Tyler[6], Antje Heese[5], Eugenia Russinova[3,4], Ping He[1,2]✉ & Libo Shan[2,9]✉

Recognition of microbe-associated molecular patterns (MAMPs) by pattern recognition receptors (PRRs) triggers the first line of inducible defence against invading pathogens[1–3]. Receptor-like cytoplasmic kinases (RLCKs) are convergent regulators that associate with multiple PRRs in plants[4]. The mechanisms that underlie the activation of RLCKs are unclear. Here we show that when MAMPs are detected, the RLCK *BOTRYTIS*-INDUCED KINASE 1 (BIK1) is monoubiquitinated following phosphorylation, then released from the flagellin receptor FLAGELLIN SENSING 2 (FLS2)–BRASSINOSTEROID INSENSITIVE 1-ASSOCIATED KINASE 1 (BAK1) complex, and internalized dynamically into endocytic compartments. The *Arabidopsis* E3 ubiquitin ligases RING-H2 FINGER A3A (RHA3A) and RHA3B mediate the monoubiquitination of BIK1, which is essential for the subsequent release of BIK1 from the FLS2–BAK1 complex and activation of immune signalling. Ligand-induced monoubiquitination and endosomal puncta of BIK1 exhibit spatial and temporal dynamics that are distinct from those of the PRR FLS2. Our study reveals the intertwined regulation of PRR–RLCK complex activation by protein phosphorylation and ubiquitination, and shows that ligand-induced monoubiquitination contributes to the release of BIK1 family RLCKs from the PRR complex and activation of PRR signalling.

Prompt activation of PRRs upon microbial infection is essential for hosts to defend against pathogen attacks[1–3]. The *Arabidopsis* BIK1 family of RLCKs are immune regulators associated with multiple PRRs, including the bacterial flagellin receptor FLS2 and the BAK1 and SERK family co-receptors[5,6]. Upon ligand perception, BIK1 is phosphorylated by BAK1 and subsequently dissociates from the FLS2–BAK1 complex[7]. Downstream of the PRR complex, BIK1 phosphorylates plasma-membrane-resident NADPH oxidases to regulate the production of reactive oxygen species (ROS)[8,9], and phosphorylates the cyclic nucleotide-gated channels to trigger a rise in cytosolic calcium[10]. However, it remains unclear how the activation of BIK1 and its dynamic association with the PRR complex is regulated.

Ligand-induced increase in BIK1 puncta

BIK1–GFP localized both to the periphery of epidermal pavement cells and to intracellular puncta in *Arabidopsis* transgenic plants expressing functional *35S::BIK1-GFP* analysed by spinning disc confocal microscopy (SDCM) (Fig. 1a, Extended Data Fig. 1a, b). BIK1–GFP colocalized with the FM4-64-stained plasma membrane (Fig. 1b), and frequently within endosomal compartments (Fig. 1b). Time-lapse SDCM showed that BIK1–GFP puncta were highly mobile, disappearing, appearing, and moving rapidly in and out of the plane of view (Extended Data Fig. 1c). The abundance of BIK1–GFP puncta increased over time (3–17 and 18–32 min) after treatment with the flagellin peptide flg22 (Fig. 1c, Extended Data Fig. 1d–p). The timing of the ligand-induced increase in BIK1–GFP puncta differed from that of the increase in FLS2–GFP puncta, which were significantly increased 35 min after flg22 treatment[11–13] (Fig. 1d). Ligand-induced endocytosis of FLS2 contributes to the degradation of the activated FLS2 receptor and attenuation of signalling[11–14], whereas increased abundance of BIK1–GFP puncta precedes that of FLS2–GFP (Fig. 1c, d).

Ligand-induced BIK1 monoubiquitination

Ligand-induced FLS2 degradation is mediated by the U-box E3 ligases PUB12 and PUB13, which polyubiquitinate FLS2[15–17]. We tested whether BIK1 is ubiquitinated upon treatment with flg22 using an in vivo ubiquitination assay in *Arabidopsis* protoplasts that co-expressed FLAG epitope-tagged ubiquitin (FLAG–UBQ) and haemagglutinin (HA)

[1]Department of Biochemistry and Biophysics, Texas A&M University, College Station, TX, USA. [2]Institute for Plant Genomics and Biotechnology, Texas A&M University, College Station, TX, USA. [3]Department of Plant Biotechnology and Bioinformatics, Ghent University, Ghent, Belgium. [4]Center for Plant Systems Biology, VIB, Ghent, Belgium. [5]Department of Biochemistry, Interdisciplinary Plant Group, University of Missouri-Columbia, Columbia, MO, USA. [6]Center for Genome Research and Biocomputing and Department of Botany and Plant Pathology, Oregon State University, Corvallis, OR, USA. [7]Department of Structural Biology, Center for Proteomics and Metabolomics, St Jude Children's Research Hospital, Memphis, TN, USA. [8]Department of Developmental Neurobiology, Center for Proteomics and Metabolomics, St Jude Children's Research Hospital, Memphis, TN, USA. [9]Department of Plant Pathology and Microbiology, Texas A&M University, College Station, TX, USA. [10]Present address: Elemental Enzymes, St Louis, MO, USA. [11]These authors contributed equally: Michelle E. Leslie, Kai Tao, Zhiping Wu. ✉e-mail: pinghe@tamu.edu; lshan@tamu.edu

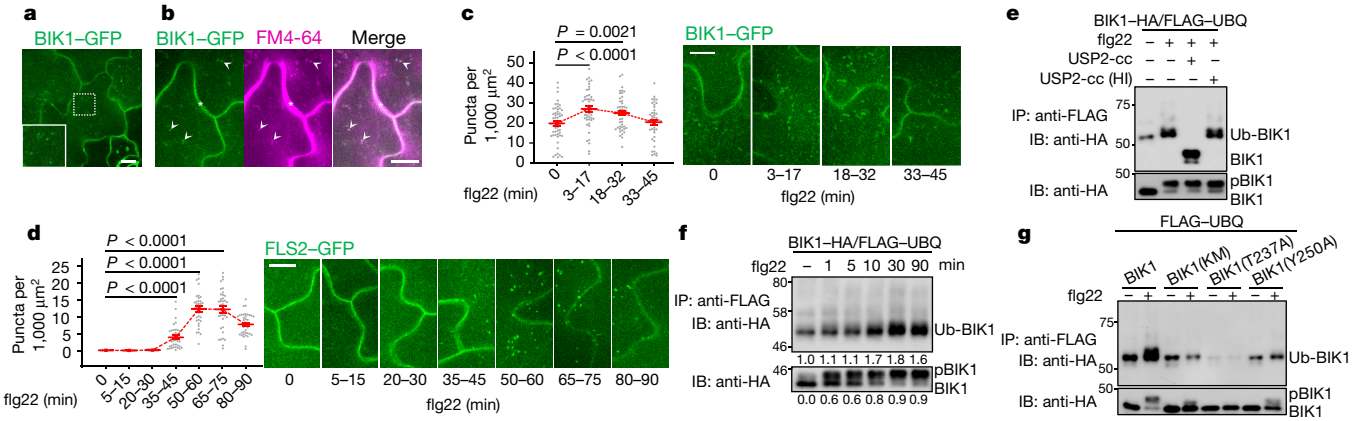

Fig. 1 | MAMP-induced BIK1 endocytosis and monoubiquitination. **a**, BIK1–GFP localizes to the cell periphery and intracellular puncta in maximum intensity projections of cotyledon epidermal cells (dashed box expanded in insert). Scale bar, 10 µm. **b**, BIK1–GFP colocalizes with FM4-64 in the plasma membrane (asterisk) and intracellular puncta (arrowheads). Scale bar, 5 µm. Pearson's correlation coefficient for BIK1–GFP and FM4-64 is 0.55 ± 0.14 (n = 35). **c**, **d**, BIK1 and FLS2 puncta increase after treatment with 1 µM flg22. Mean ± s.e.m. overlaid on dot plots. n = 56, 48, 49, 47 images for 0, 3–17, 18–32, 33–45 min of treatment, respectively, for BIK1–GFP (**c**) and n = 24, 15, 21, 36, 34, 39, 39 images for 0, 5–15, 20–30, 35–45, 50–60, 65–75, 80–90 min of treatment, respectively, for FLS2–GFP (**d**). Scale bar, 5 µm (one-way analysis of variance (ANOVA)). **e**, Flg22 induces BIK1 monoubiquitination. Protoplasts from wild-type plants were transfected with plasmids expressing *BIK1-HA* and *FLAG-UBQ*, and were treated with 100 nM flg22 for 30 min. After immunoprecipitation (IP) with anti-FLAG agarose, ubiquitinated BIK1 was detected by immunoblot (IB) using anti-HA antibodies (lanes 1 and 2) or treated with GST–USP2-cc (lane 3). Heat-inactivated (HI) USP2-cc was used as a control (lane 4). Bottom panel shows BIK1–HA protein expression. Numbers on left show molecular mass (kDa). **f**, Time-course of flg22-induced BIK1 phosphorylation and ubiquitination. Protoplasts expressing FLAG–UBQ and BIK1–HA were treated with 100 nM flg22 for the indicated times. BIK1 band intensities were quantified using Image Lab (Bio-Rad). Quantification of BIK1 phosphorylation (under bottom panel) calculated as ratio of intensity of the upper band (pBIK1) to the sum intensities of shifted and non-shifted bands (pBIK1 + BIK1). Quantification of BIK1 ubiquitination (under top panel) calculated as relative intensity (fold change) of Ub–BIK1 bands (no treatment set to 1.0). **g**, BIK1 variants with impaired phosphorylation show compromised flg22-induced ubiquitination. All experiments were repeated at least three times with similar results.

epitope-tagged BIK1 (Fig. 1e, Extended Data Fig. 2a). Treatment with flg22 induced ubiquitination of BIK1 (Fig. 1e), as ubiquitinated BIK1 was detected by an anti-HA immunoblot upon immunoprecipitation with an anti-FLAG antibody. Flg22 also induced ubiquitination of BIK1 in *pBIK1::BIK1-HA* transgenic plants (Extended Data Fig. 2b). The strong and discrete band of ubiquitinated BIK1 indicates monoubiquitination (Fig. 1e, Extended Data Fig. 2a, b), in contrast to the ladder-like smear of protein migration that indicates polyubiquitination of BAK1 and FLS2 (Extended Data Fig. 2c, d). The apparent molecular mass of ubiquitinated BIK1 (about 52 kDa) is around 8 kDa larger than that of unmodified BIK1 (44 kDa), consistent with the attachment of a single ubiquitin to BIK1. Incubation with the catalytic domain of the mouse deubiquitinase USP2 (USP2-cc), but not its heat-inactivated form, reduced the molecular mass by about 8 kDa (Fig. 1e). We observed a similar pattern of ubiquitination of BIK1 when we used the UBQ(K0) variant, in which all seven lysine residues in UBQ were changed to arginine, thus preventing the formation of polyubiquitination chains (Extended Data Fig. 2e, f). Notably, flg22-induced ubiquitination of BIK1 was blocked by treatment with the ubiquitination inhibitor PYR-41, but not by the proteasome inhibitor MG132, and was not observed in *fls2* or *bak1-4* mutants (Extended Data Fig. 2g–i). In addition to flg22, other MAMPs—including elf18, pep1, and chitin—also induced monoubiquitination of BIK1 (Extended Data Fig. 2j), in line with the notion that BIK1 is a convergent component downstream of multiple PRRs[4]. Monoubiquitination of the BIK1 family RLCKs PBL1 and PBL10, but not of another RLCK, BSK1, was enhanced upon treatment with flg22 (Extended Data Fig. 2k, l), suggesting that detection of MAMPs induces monoubiquitination of BIK1 family RLCKs.

Upon flg22 perception, BIK1 is phosphorylated[5,6], as shown by an immunoblot mobility shift within 1 min with a plateau around 10 min (Fig. 1f). However, flg22-induced ubiquitination of BIK1 becomes apparent only 10 min after treatment and reaches a plateau around 30 min (Fig. 1f), suggesting that flg22-induced ubiquitination of BIK1 may occur after its phosphorylation. BIK1 phosphorylation-deficient mutants, including a kinase-inactive mutant (BIK1(KM)) and two phosphorylation site mutants (BIK1(T237A) and BIK1(Y250A)) showed largely compromised flg22-induced ubiquitination (Fig. 1g). In addition, the kinase inhibitor K252a blocked flg22-induced ubiquitination of BIK1 (Extended Data Fig. 3a). Plasma membrane localization is required for BIK1 ubiquitination, as BIK1(G2A), which bears a mutation of the myristoylation motif that is essential for plasma membrane localization, was not ubiquitinated upon flg22 treatment (Extended Data Fig. 3b, c). Together, these data suggest that flg22-induced phosphorylation of BIK1 is a prerequisite for its monoubiquitination at the plasma membrane.

BIK1 ubiquitination by RHA3A and RHA3B

There are 30 lysine residues in BIK1, each of which could potentially be ubiquitinated. We individually mutated 28 lysine residues to arginine (except for K105 and K106, which are located in the ATP-binding pocket and are required for kinase activity), and screened the mutants for flg22-induced ubiquitination. None of the individual K-to-R mutants blocked the ubiquitination of BIK1 without altering its kinase activity (Extended Data Fig. 3d). BIK1(K204R), in which flg22-induced BIK1 monoubiquitination was compromised, also showed reduced phosphorylation in vivo and in vitro (Extended Data Fig. 3d, e). To identify BIK1-associated regulators, we carried out a yeast two-hybrid screen using BIK1(G2A) as bait, and identified *RHA3A* (*AT2G17450*), which encodes a functionally uncharacterized E3 ubiquitin ligase with a RING-H2 finger domain and an N-terminal transmembrane domain (Fig. 2a). We confirmed that BIK1 interacts with RHA3A using an in vitro pull-down assay (Fig. 2b), an in vivo co-immunoprecipitation (co-IP) assay in *Arabidopsis* protoplasts (Extended Data Fig. 4a), and co-IP in transgenic plants that expressed both *BIK1* and *RHA3A* under their native promoters (Fig. 2c, Extended Data Fig. 4b). RHA3B (which is encoded

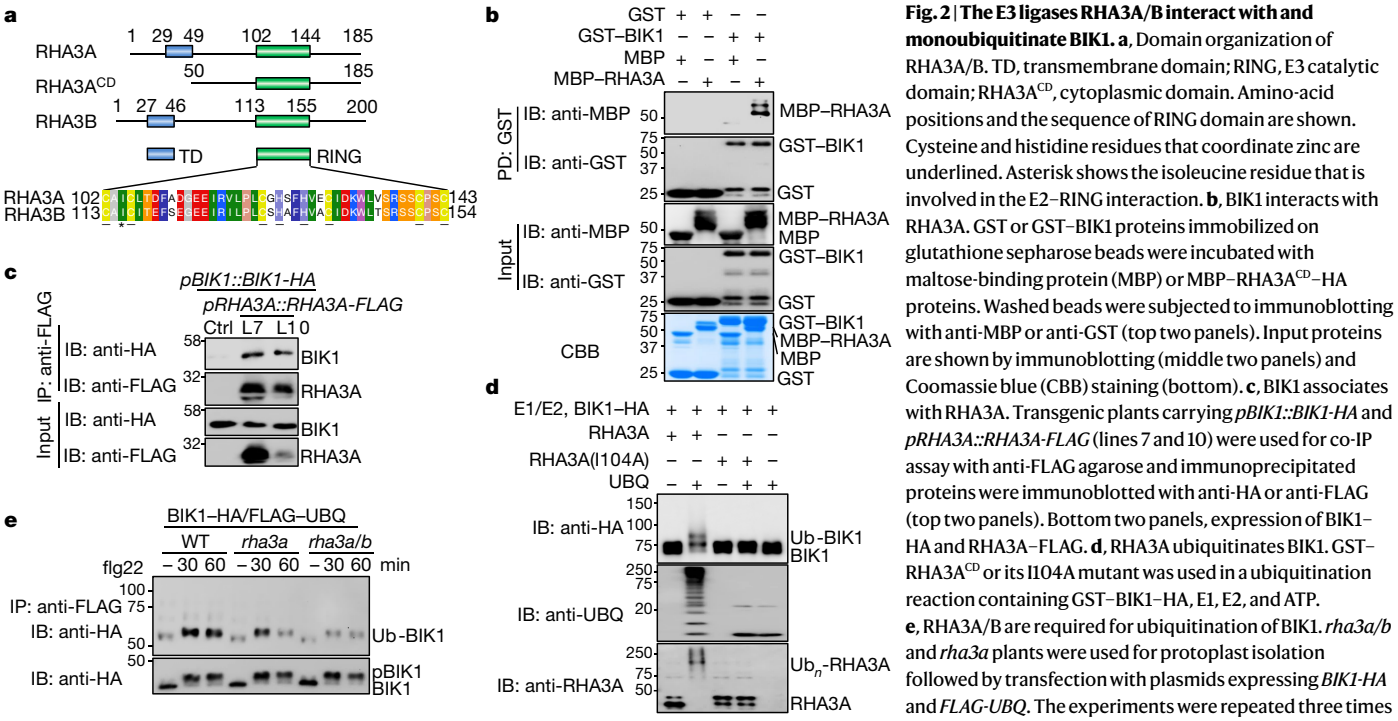

Fig. 2 | The E3 ligases RHA3A/B interact with and monoubiquitinate BIK1. a, Domain organization of RHA3A/B. TD, transmembrane domain; RING, E3 catalytic domain; RHA3A^{CD}, cytoplasmic domain. Amino-acid positions and the sequence of RING domain are shown. Cysteine and histidine residues that coordinate zinc are underlined. Asterisk shows the isoleucine residue that is involved in the E2–RING interaction. **b**, BIK1 interacts with RHA3A. GST or GST–BIK1 proteins immobilized on glutathione sepharose beads were incubated with maltose-binding protein (MBP) or MBP–RHA3A^{CD}–HA proteins. Washed beads were subjected to immunoblotting with anti-MBP or anti-GST (top two panels). Input proteins are shown by immunoblotting (middle two panels) and Coomassie blue (CBB) staining (bottom). **c**, BIK1 associates with RHA3A. Transgenic plants carrying *pBIK1::BIK1-HA* and *pRHA3A::RHA3A-FLAG* (lines 7 and 10) were used for co-IP assay with anti-FLAG agarose and immunoprecipitated proteins were immunoblotted with anti-HA or anti-FLAG (top two panels). Bottom two panels, expression of BIK1–HA and RHA3A–FLAG. **d**, RHA3A ubiquitinates BIK1. GST–RHA3A^{CD} or its I104A mutant was used in a ubiquitination reaction containing GST–BIK1–HA, E1, E2, and ATP. **e**, RHA3A/B are required for ubiquitination of BIK1. *rha3a/b* and *rha3a* plants were used for protoplast isolation followed by transfection with plasmids expressing *BIK1-HA* and *FLAG-UBQ*. The experiments were repeated three times with similar results.

by *AT4G35480*) is the closest homologue of RHA3A, bearing 66% amino acid identity (Fig. 2a); RHA3B also co-immunoprecipitated with BIK1 (Extended Data Fig. 4c). Flg22 treatment did not affect the interaction between BIK1 and RHA3A or RHA3B (called RHA3A/B henceforth) (Extended Data Fig. 4a, c). Moreover, RHA3A/B co-immunoprecipitated with FLS2 (Extended Data Fig. 4d).

An in vitro ubiquitination assay showed that RHA3A had autoubiquitination activity and monoubiquitinated itself (Extended Data Fig. 5a, b). Notably, glutathione-*S*-transferase (GST)–RHA3A, but not GST–RHA3A(I104A), in which a conserved isoleucine residue had been substituted, monoubiquitinated GST–BIK1–HA, as shown on immunoblots by an additional discrete band that migrated with an approximately 8-kDa increase in molecular mass (Fig. 2d). The available *rha3a* and *rha3b* transfer DNA (T-DNA) insertion lines did not show a significant reduction in expression of the corresponding transcripts (Extended Data Fig. 5c). We therefore generated artificial microRNAs (amiRNAs) of *RHA3A/B*[18]. Co-expression of *amiR-RHA3A* and *amiR-RHA3B*, but not of *amiR-RHA3A* alone, suppressed flg22-induced monoubiquitination of BIK1 in protoplast transient assays (Extended Data Fig. 5d, e). Flg22-induced BIK1 monoubiquitination, but not phosphorylation, was also reduced in transgenic plants expressing *amiR-RHA3A* and *amiR-RHA3B* driven by the native promoters (Extended Data Fig. 5f, g). We also generated *rha3a* and *rha3a/b* mutants using the CRISPR–Cas9 system (Extended Data Fig. 5h). Flg22-induced monoubiquitination of BIK1 was reduced in the *rha3a/b* mutant (Fig. 2e). These data indicate that RHA3A/B modulate flg22-induced monoubiquitination of BIK1.

Sites of RHA3A-mediated BIK1 ubiquitination

To identify sites of RHA3A-mediated BIK1 ubiquitination, we performed liquid chromatography-tandem mass spectrometry (LC–MS/MS) analysis of in vitro ubiquitinated BIK1. Among ten lysine residues identified (Fig. 3a, b,Extended Data Fig. 6a–i), K106 (which resides in the ATP-binding pocket) blocked BIK1 kinase activity when mutated[7]. Among the other nine lysine sites, all six lysines (K95, K170, K186, K286, K337, and K358) for which structural information is available[19] are located on the surface of BIK1 (Fig. 3c). Furthermore, six ubiquitinated lysine residues were detected by LC–MS/MS of in vivo ubiquitinated BIK1–GFP upon treatment with flg22, and they all overlapped with those detected during in vitro RHA3A–BIK1 ubiquitination reactions (Extended Data Fig. 7a–h). Individual lysine mutations did not affect ubiquitination of BIK1 in vivo (Extended Data Fig. 3d), whereas combined mutations of the N-terminal five lysines (BIK1(N5KR)) or C-terminal four lysines (BIK1(C4KR)) partially compromised flg22-induced BIK1 ubiquitination. Mutation of all nine lysines in BIK1(9KR) largely blocked flg22-induced BIK1 monoubiquitination in vivo (Fig. 3d) and RHA3A-mediated in vitro ubiquitination (Fig. 3e). BIK1(9KR) showed similar activities to BIK1 with regard to its in vitro kinase activity (Fig. 3f), flg22-induced BIK1 phosphorylation, and association with RHA3A in protoplasts (Extended Data Fig. 8a, b). Furthermore, *35S::BIK1^{9KR}-HA*/WT transgenic plants showed normal flg22-induced MAPK activation and ROS production (Extended Data Fig. 8c, d). Collectively, the data indicate that RHA3A monoubiquitinates BIK1 and that phosphorylation of BIK1 does not require monoubiquitination. Notably, BIK1 monoubiquitination may not be restricted to a single lysine, and multiple lysine residues could serve as monoubiquitin conjugation sites. Alternatively, monoubiquitination might be the primary form of modification of BIK1, whereas polyubiquitinated BIK1 could be short-lived.

BIK1 monoubiquitination in immunity

BIK1(9KR), in which monoubiquitination but not phosphorylation of BIK1 is blocked, enabled us to examine the function of BIK1 monoubiquitination without compromised kinase activity. We generated *BIK1^{9KR}* transgenic plants driven by the *BIK1* native promoter in a *bik1* background (*pBIK1::BIK1^{9KR}-HA/bik1*) (Extended Data Fig. 8e, f). Unlike *pBIK1::BIK1-HA/bik1* transgenic plants, *pBIK1::BIK1^{9KR}-HA/bik1* transgenic plants exhibited a reduced flg22-triggered ROS burst similar to that of the *bik1* mutant (Fig. 4a). Moreover, *pBIK1::BIK1^{9KR}-HA/bik1* transgenic plants were more susceptible to the bacterial pathogen *Pseudomonas syringae* pv. *tomato* (*Pst*) DC3000 *hrcC*$^-$ than were wild-type or *pBIK1::BIK1-HA/bik1* transgenic plants (Fig. 4b). In addition, *amiR-RHA3A/B* transgenic plants exhibited compromised

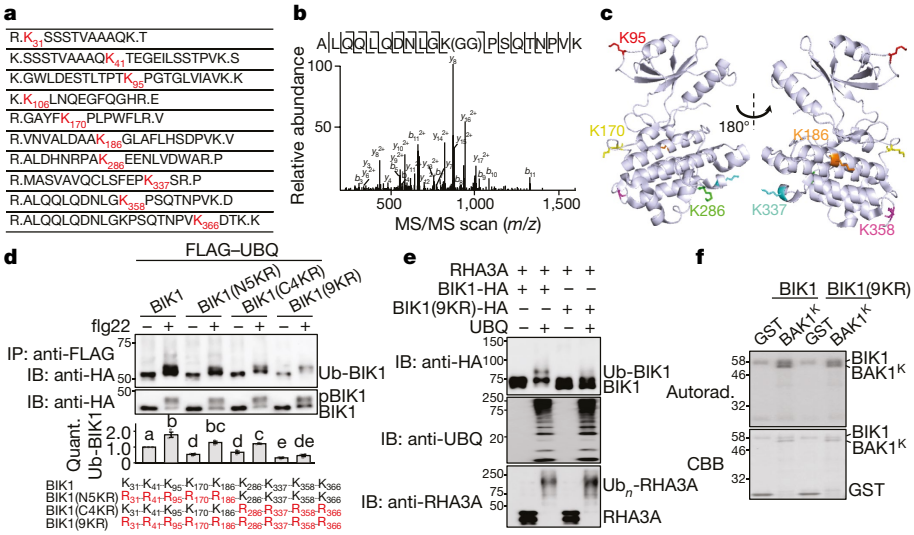

Fig. 3 | Identification of sites of RHA3A-mediated BIK1 ubiquitination. **a**, BIK1 is ubiquitinated by RHA3A at multiple lysine residues. Ubiquitinated lysine residues with a diglycine remnant identified by LC–MS/MS analysis are shown in red with amino-acid positions. **b**, MS/MS spectrum of the peptide containing K_{358}. **c**, Structure of BIK1 with six lysines identified as ubiquitination sites shown. Structural information was obtained from the Protein Data Bank (PDB ID: 5TOS) and analysed by PyMOL. **d**, BIK1(9KR) shows compromised flg22-induced ubiquitination. FLAG–UBQ and HA-tagged BIK1 mutants were expressed in protoplasts followed by treatment with 100 nM flg22 for 30 min. Quantification of fold change in BIK1 ubiquitination is shown mean ± s.e.m. overlaid on dot plot (middle). Different letters indicate significant difference with others (for example, the rightmost bar is significantly different from those marked a, b, and c but not d or e) ($P < 0.05$, one-way ANOVA, $n = 3$). Lysines mutated in BIK1 mutants are shown in red (bottom). **e**, RHA3A cannot ubiquitinate BIK1(9KR). The assay was performed as in Fig. 2d. **f**, BIK1(9KR) exhibits normal in vitro kinase activity. The kinase assay was performed using GST–BIK1 or GST–BIK1(9KR) as the kinase and GST or GST–BAK1^K (kinase domain) as the substrate. All experiments except MS analyses were repeated three times with similar results.

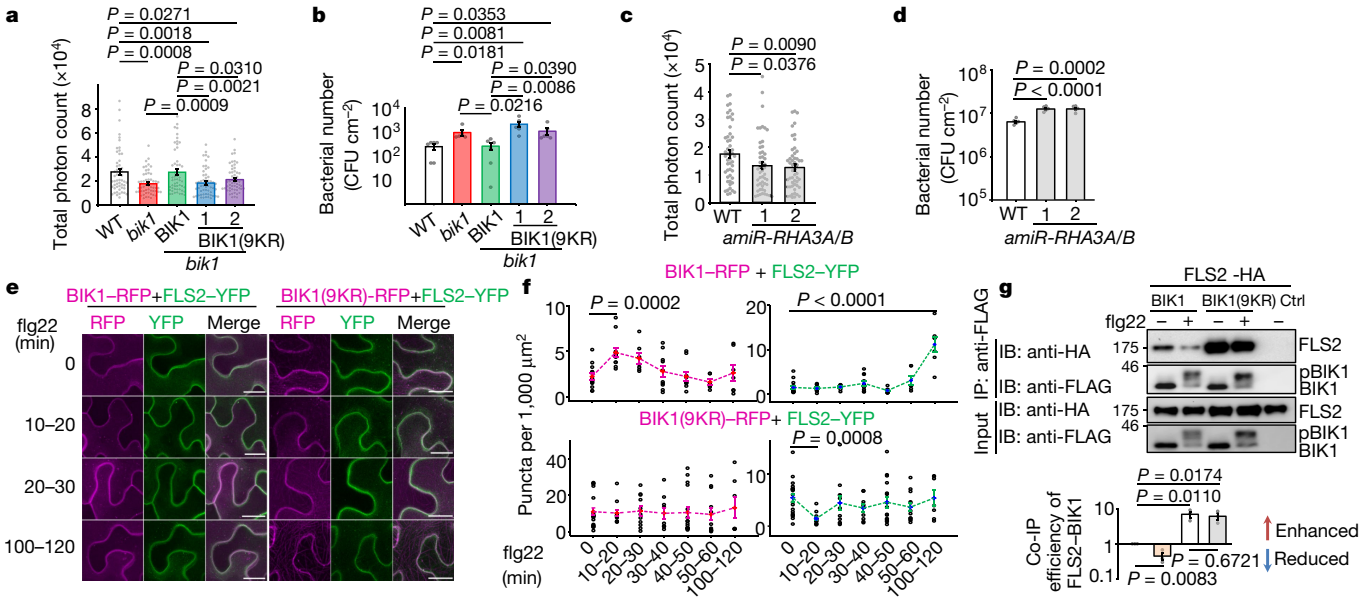

Fig. 4 | RHA3A/B-mediated monoubiquitination of BIK1 contributes to its function in immunity and endocytosis. **a**, *pBIK1::BIK1^{9KR}-HA/bik1* transgenic plants (lines 1 and 2) cannot complement *bik1* for flg22-induced ROS production. One-way ANOVA; wild-type, BIK1/*bik1*: $n = 53$; *bik1*: $n = 54$; BIK1(9KR)/*bik1*: $n = 55$. In all panels, data are shown as mean ± s.e.m. overlaid on dot plot; lines beneath *P* values indicate relevant pairwise comparisons. **b**, The *pBIK1::BIK1^{9KR}-HA/bik1* transgenic plants show increased bacterial growth of *Pst* DC3000 *hrcC*$^-$. Plants were spray-inoculated and bacterial growth was measured at four days post-inoculation (dpi). One-way ANOVA, $n = 6$. CFU, colony-forming units. **c**, *amiRNA-RHA3A/B* plants show reduced flg22-induced ROS production. One-way ANOVA, $n = 51$. **d**, *amiRNA-RHA3A/B* plants show increased bacterial growth of *Pst* DC3000. Plants were hand-inoculated and bacterial growth was measured at 2 dpi. One-way ANOVA, $n = 5$. **e**, **f**, Flg22-induced endocytosis of BIK1, BIK1(9KR), and FLS2 in *N. benthamiana* leaf epidermal cells. **e**, BIK1–TagRFP or BIK1(9KR)–TagRFP was co-expressed with FLS2–YFP followed by treatment with 100 µM flg22 and then imaged at the indicated time points by confocal microscopy. Scale bars, 20 µm. **f**, Quantification of BIK1–TagRFP (magenta) and FLS2–YFP (green) puncta. One-way ANOVA, additional images and *n* values shown in Extended Data Fig. 9c. **g**, BIK1(9KR) does not enable flg22-induced dissociation of BIK1 from FLS2. Top, co-IP was performed using protoplasts expressing FLS2–HA and BIK1–FLAG or BIK1(9KR)–FLAG, followed by treatment with 1 µM flg22 for 15 min. Bottom, the interaction of BIK1 with FLS2 was quantified as intensity from IP: anti-FLAG, IB: anti-HA divided by intensity from IP: anti-FLAG, IB: anti-FLAG. Mean ± s.e.m. fold change (BIK1 no treatment = 1.0; one-way ANOVA, $n = 3$). All experiments were repeated three times with similar results.

flg22-triggered production of ROS and enhanced susceptibility to *Pst* DC3000 (Fig. 4c, d) and *Pst* DC3000 *hrcC*$^-$ and to the fungal pathogen *Botrytis cinerea* (Extended Data Fig. 8g, h). Similar results were obtained with the *rha3a/b* mutants (Extended Data Fig. 8i, j). Together, the data indicate that RHA3A/B-mediated monoubiquitination of BIK1 has a role in regulating ROS production and plant immunity.

BIK1 monoubiquitination in endocytosis

As detection of flg22 moderately increased BIK1–GFP endosomal puncta (Fig. 1c), we tested whether monoubiquitination of BIK1 is involved in flg22-triggered BIK1 endocytosis. Fewer FM4-64-labelled puncta were observed in plants expressing BIK1(9KR)–GFP than in those expressing BIK1–GFP after 10 or 15 min of treatment with flg22 (Extended Data Fig. 9a, b). In addition, we compared the flg22-triggered endocytosis of BIK1–TagRFP and BIK1(9KR)–TagRFP when co-expressed with FLS2–YFP in *Nicotiana benthamiana*. As seen in transgenic plants (Fig. 1c, d), endosomal puncta of BIK1–TagRFP increased at 10–20 min, whereas FLS2–YFP puncta increased only after 60 min of flg22 treatment (Fig. 4e, f, Extended Data Fig. 9c). A large portion (about 90%) of flg22-induced BIK1–TagRFP puncta did not colocalize with FLS2–YFP puncta (Extended Data Fig. 9d), suggesting that BIK1 and FLS2 are not likely to be internalized together. This is consistent with the differing ubiquitination characteristics of BIK1 and FLS2 (monoubiquitination versus polyubiquitination, 10 min versus 1 h). When compared to BIK1, BIK1(9KR)–TagRFP was more abundant in puncta before treatment, but the number of puncta did not increase after flg22 treatment (Fig. 4e, f, Extended Data Fig. 9c), indicating that internalization of BIK1(9KR)–TagRFP does not respond to activation of PRRs. In addition, colocalization of BIK1(9KR)–TagRFP with YFP-tagged ARA6 (a plant-specific Rab GTPase that resides on late endosomes[20]) was substantially reduced when compared to that of BIK1–TagRFP (Extended Data Fig. 9e, f). Notably, flg22-induced endocytosis of FLS2–YFP was absent in the presence of BIK1(9KR)–TagRFP (Fig. 4e, f). Together, our data support the conclusion that ligand-induced monoubiquitination of BIK1 contributes to its internalization from the plasma membrane. Notably, whereas flg22 treatment induced phosphorylation-dependent dissociation of BIK1 from FLS2[5,6,21], this effect was largely absent in the case of BIK1(9KR) (Fig. 4g), consistent with the finding that BIK1(9KR) shows impaired FLS2 internalization (Fig. 4e, f). In addition, we observed an increase in the association between BIK1(9KR) and FLS2 without flg22 treatment (Fig. 4g). Treatment with the ubiquitination inhibitor PYR-41 also blocked flg22-induced dissociation of BIK1 from FLS2 and enhanced BIK1–FLS2 association (Extended Data Fig. 10a). Our data indicate that ligand-induced monoubiquitination of BIK1 has an important role in dissociation of BIK1 from the plasma membrane-localized PRR complex, endocytosis of BIK1 and activation of immune signalling (Extended Data Fig. 10b).

Discussion

The BIK1 family RLCKs are central elements of plant PRR signalling, with many layers of regulation[4,22]. The stability of BIK1 is crucial for maintaining immune homeostasis. The plant U-box proteins PUB25 and PUB26 polyubiquitinate BIK1 and regulate its stability in the steady state[23]. This module regulates the homeostasis of non-activated BIK1 without affecting ligand-activated BIK1[23]. We have identified a role of RHA3A/B in monoubiquitinating BIK1 and activating PRR signalling, which is distinct from that of PUB25 and PUB26. The levels of BIK1(9KR) proteins in transgenic plants and protoplasts are similar to those of wild-type BIK1 (Extended Data Fig. 10c, d), suggesting that monoubiquitination of BIK1 may not regulate its stability. The nature of protein ubiquitination, including monoubiquitination and polyubiquitination, dictates the distinct fates of substrates, such as proteasome-mediated protein degradation, nonproteolytic functions of protein kinase activation, and membrane trafficking[24]. Ligand-induced polyubiquitination of FLS2 by PUB12 or PUB13 promotes degradation of FLS2, thereby attenuating immune signalling[15,16], whereas ligand-induced monoubiquitination of BIK1 triggers dissociation of BIK1 from PRR complexes and activates intracellular signalling. Thus, differential ubiquitination and endocytosis of distinct PRR–RLCK complex components are likely to serve as cues to fine-tune plant immune responses.

Online content

Any methods, additional references, Nature Research reporting summaries, source data, extended data, supplementary information, acknowledgements, peer review information; details of author contributions and competing interests; and statements of data and code availability are available at https://doi.org/10.1038/s41586-020-2210-3.

1. Couto, D. & Zipfel, C. Regulation of pattern recognition receptor signalling in plants. *Nat. Rev. Immunol.* **16**, 537–552 (2016).
2. Yu, X., Feng, B., He, P. & Shan, L. From chaos to harmony: responses and signaling upon microbial pattern recognition. *Annu. Rev. Phytopathol.* **55**, 109–137 (2017).
3. Spoel, S. H. & Dong, X. How do plants achieve immunity? Defence without specialized immune cells. *Nat. Rev. Immunol.* **12**, 89–100 (2012).
4. Liang, X. & Zhou, J. M. Receptor-like cytoplasmic kinases: central players in plant receptor kinase-mediated signaling. *Annu. Rev. Plant Biol.* **69**, 267–299 (2018).
5. Lu, D. et al. A receptor-like cytoplasmic kinase, BIK1, associates with a flagellin receptor complex to initiate plant innate immunity. *Proc. Natl Acad. Sci. USA* **107**, 496–501 (2010).
6. Zhang, J. et al. Receptor-like cytoplasmic kinases integrate signaling from multiple plant immune receptors and are targeted by a *Pseudomonas syringae* effector. *Cell Host Microbe* **7**, 290–301 (2010).
7. Lin, W. et al. Tyrosine phosphorylation of protein kinase complex BAK1/BIK1 mediates *Arabidopsis* innate immunity. *Proc. Natl Acad. Sci. USA* **111**, 3632–3637 (2014).
8. Li, L. et al. The FLS2-associated kinase BIK1 directly phosphorylates the NADPH oxidase RbohD to control plant immunity. *Cell Host Microbe* **15**, 329–338 (2014).
9. Kadota, Y. et al. Direct regulation of the NADPH oxidase RBOHD by the PRR-associated kinase BIK1 during plant immunity. *Mol. Cell* **54**, 43–55 (2014).
10. Tian, W. et al. A calmodulin-gated calcium channel links pathogen patterns to plant immunity. *Nature* **572**, 131–135 (2019).
11. Smith, J. M. et al. Loss of *Arabidopsis thaliana* Dynamin-Related Protein 2B reveals separation of innate immune signaling pathways. *PLoS Pathog.* **10**, e1004578 (2014).
12. Beck, M., Zhou, J., Faulkner, C., MacLean, D. & Robatzek, S. Spatio-temporal cellular dynamics of the *Arabidopsis* flagellin receptor reveal activation status-dependent endosomal sorting. *Plant Cell* **24**, 4205–4219 (2012).
13. Robatzek, S., Chinchilla, D. & Boller, T. Ligand-induced endocytosis of the pattern recognition receptor FLS2 in *Arabidopsis*. *Genes Dev.* **20**, 537–542 (2006).
14. Smith, J. M., Salamango, D. J., Leslie, M. E., Collins, C. A. & Heese, A. Sensitivity to Flg22 is modulated by ligand-induced degradation and de novo synthesis of the endogenous flagellin-receptor FLAGELLIN-SENSING2. *Plant Physiol.* **164**, 440–454 (2014).
15. Lu, D. et al. Direct ubiquitination of pattern recognition receptor FLS2 attenuates plant innate immunity. *Science* **332**, 1439–1442 (2011).
16. Zhou, J. et al. The dominant negative ARM domain uncovers multiple functions of PUB13 in *Arabidopsis* immunity, flowering, and senescence. *J. Exp. Bot.* **66**, 3353–3366 (2015).
17. Zhou, J. et al. Regulation of *Arabidopsis* brassinosteroid receptor BRI1 endocytosis and degradation by plant U-box PUB12/PUB13-mediated ubiquitination. *Proc. Natl Acad. Sci. USA* **115**, E1906–E1915 (2018).
18. Li, J. F., Zhang, D. & Sheen, J. Epitope-tagged protein-based artificial miRNA screens for optimized gene silencing in plants. *Nat. Protocols* **9**, 939–949 (2014).
19. Lal, N. K. et al. The receptor-like cytoplasmic kinase BIK1 localizes to the nucleus and regulates defense hormone expression during plant innate immunity. *Cell Host Microbe* **23**, 485–497.e485 (2018).
20. Ueda, T., Yamaguchi, M., Uchimiya, H. & Nakano, A. Ara6, a plant-unique novel type Rab GTPase, functions in the endocytic pathway of *Arabidopsis thaliana*. *EMBO J.* **20**, 4730–4741 (2001).
21. Lin, W. et al. Inverse modulation of plant immune and brassinosteroid signaling pathways by the receptor-like cytoplasmic kinase BIK1. *Proc. Natl Acad. Sci. USA* **110**, 12114–12119 (2013).
22. Lin, W., Ma, X., Shan, L. & He, P. Big roles of small kinases: the complex functions of receptor-like cytoplasmic kinases in plant immunity and development. *J. Integr. Plant Biol.* **55**, 1188–1197 (2013).
23. Wang, J. et al. A regulatory module controlling homeostasis of a plant immune kinase. *Mol. Cell* **69**, 493–504.e496 (2018).
24. Zhou, B. & Zeng, L. Conventional and unconventional ubiquitination in plant immunity. *Mol. Plant Pathol.* **18**, 1313–1330 (2017).

Methods

No statistical methods were used to predetermine sample size. The experiments were not randomized and the investigators were not blinded to allocation during experiments and outcome assessment.

Plant materials and growth conditions

A. thaliana accession Col-0 (wild type, WT), mutants *fls2*, *bak1-4*, *bik1*, transgenic *pBIK1::BIK1-HA* in the *bik1* background, and *pFLS2::FLS2-GFP* in the Col-0 background have been described previously[7,13]. *p35S::BIK-GFP* and *p35S::BIK1^{9KR}-GFP* in the Col-0 background, *pBIK1::BIK1^{9KR}-HA* transgenic plants in the *bik1* background, *p35S::BIK1-HA*, *p35S::BIK1^{9KR}-HA* transgenic plants in the Col-0 background, *pBIK1::BIK1-HA* in the Col-0 background, *pBIK1::BIK1-HA/pRHA3A::RHA3A-FLAG* double transgenic plants in the Col-0 background and *pRHA3A::amiR-RHA3A-pRHA3B::amiR-RHA3B* transgenic plants in the Col-0 background were generated in this study (see below). All *Arabidopsis* plants were grown in soil (Metro Mix 366, Sunshine LP5 or Sunshine LC1, Jolly Gardener C/20 or C/GP) in a growth chamber at 20–23 °C, 50% relative humidity and 75 μE m^{-2} s^{-1} light with a 12-h light/12-h dark photoperiod for four weeks before pathogen infection assay, protoplast isolation, and ROS assay. For confocal microscopy imaging, seeds were sterilized, maintained for 2 days at 4 °C in the dark, and germinated on vertical half-strength Murashige and Skoog (½MS) medium (1% (wt/vol) sucrose) agar plates, pH 5.8, at 22 °C in a 16-h light/8-h dark cycle for 5 days with a light intensity of 75 μE m^{-2} s^{-1}. For FM4-64 staining, whole seedlings were incubated for 15 min in 3 ml of ½MS liquid medium containing 2 μM FM4-64 and washed twice by dipping into deionized water before adding the elicitor (flg22, 100 nM). Wild-type tobacco (*N. benthamiana*) plants were grown under 14 h of light and 10 h of darkness at 25 °C.

Statistical analyses

Data for quantification analyses are presented as mean ± s.e.m. The statistical analyses were performed by Student's *t*-test or one-way ANOVA test. The number of replicates is given in the figure legends.

Plasmid construction and generation of transgenic plants

FLS2, BAK1, BIK1, PBL1, PBL10 or BSK1 tagged with HA, FLAG or GFP in a plant gene expression vector pHBT used for protoplast assays, and FLS2^{CD}, BAK1^{CD}, BAK1^{K}, PUB13, BIK1, or BIK1(KM) fused with GST or MBP used for *Escherichia coli* fusion protein isolation have been described previously[5,7]. BIK1 point mutations in a *pHBT* vector were generated by site-directed mutagenesis with primers listed in Supplementary Table 1 using the *pHBT-BIK1-HA* construct as the template. *BIK1^{N5KR}* was constructed by sequentially mutating K41, K95, K170 and K186 into arginine on *BIK1^{K31R}*. *BIK1^{C4KR}* was constructed by sequentially mutating K337, K358 and K366 on *BIK1^{K286R}*. *pHBT-BIK1^{N5KR}* and *pHBT-BIK1^{C4KR}* were then digested with XbaI and StuI and ligated together to generate *pHBT-BIK1^{9KR}-HA*. *BIK1^{9KR}* was sub-cloned into *pHBT-FLAG* or *pHBT-GFP* with BamHI and StuI digestion to generate *pHBT-BIK1^{9KR}-FLAG* or *pHBT-BIK1^{9KR}-GFP*. *BIK1^{9KR}* was sub-cloned into the binary vector *pCB302-pBIK1::BIK1-HA* or *pCB302-35S::BIK1-HA* with BamHI and StuI digestion to generate *pCB302-pBIK1::BIK1^{9KR}-HA*, or *pCB302-35S::BIK1^{9KR}-HA*. *BIK1-GFP* or *BIK1^{9KR}-GFP* was sub-cloned into *pCB302* with BamHI and PstI digestion to generate *pCB302-35S::BIK1-GFP* and *pCB302-35S::BIK1^{9KR}-GFP*. *BIK1^{K204R}* or *BIK1^{9KR}* was sub-cloned into a modified GST (*pGEX4T-1*, Pharmacia) vector with BamHI and StuI digestion to generate *pGST-BIK1^{K204R}* or *pGST-BIK1^{9KR}*, respectively. *BIK1-HA* or *BIK1^{9KR}-HA* was further sub-cloned into the *pGST* vector as following: digestion with PstI, blunting end by T4 DNA polymerase, digestion with BamHI and ligation into a BamHI/StuI-digested *pGST* vector to generate *pGST-BIK1-HA* and *pGST-BIK1^{9KR}-HA*.

The *RHA3A* gene (*AT2G17450*) was cloned by PCR amplification from Col-0 complementary (c)DNAs with primers containing BamHI at the 5′ end and StuI at the 3′ end, followed by BamHI and StuI digestion and ligation into the *pHBT* vector with an HA or FLAG tag at the C terminus. The *RHA3B* gene (*AT4G35480*) was cloned similarly to *RHA3A* using BamHI and SmaI-containing primers. *pHBT-RHA3A^{I104A}* was generated by site-directed mutagenesis with primers listed in Supplementary Table 1. *RHA3A^{CD}* (amino acids 50–186) and *RHA3A$^{CD/I104A}$* were cloned by PCR amplification from *RHA3A* or *RHA3A^{I104A}*, respectively, using BamHI- and StuI-containing primers. *RHA3A^{CD}* and *RHA3A$^{CD/I104A}$* were sub-cloned into *pGST* or a modified *pMBP* (pMAL-c2, NEB) vector with BamHI and StuI digestion for isolation of *E. coli* fusion proteins. The promoter of *RHA3A* or *RHA3B* was PCR-amplified from genomic DNAs of Col-0 with primers containing SacI and BamHI, and ligated into *pHBT*. The fragment of *pRHA3A::RHA3A-FLAG* was digested by SacI and EcoRI, and ligated into *pCAMBIA2300*.

AmiRNA constructs were generated as previously described[18]. In brief, amiRNA candidates were designed according to instructions at http://wmd3.weigelworld.org/cgi-bin/webapp.cgi. Three candidates were chosen for each gene with *RHA3A* for *amiRNA480*: TTTTGTCAATACACTCCACGG; *amiRNA211*: TCAACGCAGATAAGAGCGCTA; *amiRNA109*: TCAAGTAATCTTGACGGTCGT, and *RHA3B* for *amiRNA444*: TTATGCATATTGCACACTCCG; *amiRNA113*: TAATCTAGAGGAGCGAGTCAG; *amiRNA214*: TCTACGCATACGAGAGCGCAT. Primers for cloning amiRNAs were generated according to instructions at http://wmd3.weigelworld.org/cgi-bin/webapp.cgi. The cognate fragments were cloned into the *pHBT-amiRNA-ICE1* vector[18]. *pCB302-pRHA3A::amiRNA-RHA3A-pRHA3B::amiRNA-RHA3B* was constructed as follows: the *RHA3A* promoter was PCR amplified from *pRHA3A::RHA3A-FLAG*, digested with SacI and BamHI and ligated with *pHBT-amiR-RHA3A* to generate *pHBT-pRHA3A::amiR-RHA3A*. The *pRHA3A::amiR-RHA3A* fragment was further released by SacI and PstI digestion and ligated into pCB302 vector to generate *pCB302-pRHA3A::amiRNA-RHA3A*. *pHBT-pRHA3B::amiR-RHA3B* was constructed similarly followed by PCR amplification using a primer containing SacI sites at both the 5′ and 3′ends, subsequent digestion with SacI and ligation into the *pCB302-pRHA3A::amiRNA-RHA3A* vector. Tandem *pRHA3A/B-amiRNA-RHA3A/B* in the same direction was confirmed by digestion and selected for further experiments.

The *rha3a/b* mutant was generated by the CRISPR–Cas9 system following the published protocol[25]. In brief, primers containing guide RNA (gRNA) sequences of *RHA3A* and *RHA3B* were used in PCR to insert both gRNA sequences into the *pDT1T2* vector. The *pDT1T2* vector containing both gRNAs was further PCR amplified, digested with BsaI and ligated into a binary vector *pHEE401E*. *Agrobacterium-tumefaciens*-mediated floral dip was used to transform the *pHEE401E* vector into Col-0 plants. Genomic DNAs from hygromycin (25 μg/ml)-positive plants were extracted, PCR amplified with gene-specific primers and sequenced by Sanger sequencing.

The monomer ubiquitin of *Arabidopsis* ubiquitin gene 10 (*UBQ10*, *At4g05320*) carrying lysine-to-arginine mutations at all the seven lysine residues (*UBQ^{KO}*: 5′-ATGCAGATCTTTGTTAGGACTCTCACCGGAAGGACTATCACCCTCGAGGTGGAAAGCTCTGACACCATCGACAACGTTAGGGCCAGGATCCAGGATAGGGAAGGTATTCCTCCGGATCAGCAGAGGCTTATCTTCGCCGGAAGGCAGTTGG AGGATGGCCGCACGTTGGCGGATTACAATATCCAGAGGGAATCCA CCCTCCACTTGGTCCTCAGGCTCCGTGGTGGTTAA-3′) was synthesized and cloned into a *pUC57* vector by GenScript USA Incorporation. *UBQ^{KO}* was then amplified by PCR with primers listed in the Supplementary Table 1 and further sub-cloned into a modified *pHBT* vector with BamHI and PstI digestion to generate *pHBT-FLAG-UBQ^{KO}*.

Plasmids used for transient expression in *N. benthamiana* were constructed as reported previously[26]. In brief, *FLS2*, *BIK1*, and *BIK1^{9KR}* were PCR amplified and recombined into *pDONR207-YFP*, *pDONR207-TagRFP*, and *pDONR207-GFP* vectors by In-Fusion HD Cloning (TaKaRa Bio). The *pDONR207* vectors were subsequently transferred to a destination vector *pmAEV* (derived from binary vector *pCAMBIA*

with a 35S promoter) using the Gateway LR reaction (Thermo Fisher scientific).

DNA fragments cloned into the final constructs were confirmed via Sanger sequencing. *A.-tumefaciens*-mediated floral dip was used to transform the above binary vectors into *bik1* or Col-0 plants. The transgenic plants were selected using glufosinate-ammonium (Basta, 50 μg/ml) for the *pCB302* vector or kanamycin (50 μg/ml) for the *pCAMBIA2300* vector. Multiple transgenic lines were analysed by immunoblotting for protein expression. Two lines with 3:1 segregation ratios for antibiotic resistance in the T3 generation were selected to obtain homozygous seeds for further studies. *amiR-RHA3A/B* transgenic plants that were resistant to Basta in the T2 generation were used for assays.

Yeast two-hybrid screen

The cDNA library constructed in a modified pGADT7 vector (Clontech) has been previously described[15]. BIK1(G2A) from *pHBT-BIK1^{G2A}-HA* was sub-cloned into a modified *pGBKT7* vector with BamHI and StuI digestion. *pGBK-BIK1^{G2A}* was transformed into the yeast AH109 strain. The resulting yeast transformants were then transformed with the cDNA library and screened in synthetic defined (SD) medium without Trp, Leu, His, Ade (SD-T-L-H-A) and SD-T-L-H containing 1 mM 3-amino-1, 2, 4-triazole (3-AT). The confirmed yeast colonies were subjected to plasmid isolation and sequencing.

Pathogen infection assays

Pst DC3000 was cultured overnight at 28 °C in King's B medium supplemented with rifamycin (50 μg/ml). Bacteria were collected by centrifugation at 3,000*g*, washed and re-suspended to a density of 10^6 colony-forming units (cfu)/ml with 10 mM $MgCl_2$. Leaves from four-week-old plants were hand-inoculated with bacterial suspension using a needleless syringe. To measure in planta bacterial growth, five to six sets of two leaf discs, 6 mm in diameter, were punched and ground in 100 μl ddH_2O. Serial dilutions were plated on TSA plates (1% tryptone, 1% sucrose, 0.1% glutamatic acid and 1.8% agar) containing 25 μg/ml rifamycin. Plates were incubated at 28 °C and bacterial cfu were counted 2 days after incubation. For spray inoculation, *Pst* DC3000 or *Pst* DC3000 *hrcC*$^-$ bacteria were collected and re-suspended to 5×10^8 cfu/ml with 10 mM $MgCl_2$, silwet L-77 (0.02%) and sprayed onto the leaf surface. Plants were covered with a transparent plastic dome to maintain humidity after spraying. After incubation, the third pair of true leaves was detached, soaked in 70% ethanol for 30 s and rinsed in water, and bacterial growth was measured as described above.

Protoplast transient expression and co-IP assays

Protoplast isolation and the transient expression assay have been described previously[27]. For protoplast-based co-IP assays, protoplasts were transfected with a pair of constructs (the empty vectors as controls, 100 μg DNA for 500 μl protoplasts at a density of 2×10^5/ml for each sample) and incubated at room temperature for 6–10 h. After treatment with flg22 at the indicated concentrations and time points, protoplasts were collected by centrifugation and lysed in 300 μl co-IP buffer (150 mM NaCl, 50 mM Tris-HCl, pH7.5, 5 mM EDTA, 0.5% Triton, 1 × protease inhibitor cocktail, before use, adding 2.5 μl 0.4 M DTT, 2 μl 1 M NaF and 2 μl 1 M Na_3VO_3 for 1 ml IP buffer) by vortexing. After centrifugation at 10,000*g* for 10 min at 4 °C, 30 μl supernatant was collected for input controls and 7 μl anti-FLAG–agarose beads were added to the remaining supernatant and incubated at 4 °C for 1.5 h. Beads were collected and washed three times with washing buffer (150 mM NaCl, 50 mM Tris-HCl, pH 7.5, 5 mM EDTA, 0.5% Triton) and once with 50 mM Tris-HCl, pH 7.5. Immunoprecipitates were analysed by immunoblotting with the indicated antibodies. The amiRNA candidate screens were performed as previously described[18].

In vivo ubiquitination assay

FLAG-tagged UBQ (FLAG–UBQ) or a vector control (40 μg DNA) was co-transfected with the target gene with an HA tag (40 μg DNA) into 400 μl protoplasts at a density of 2×10^5/ml for each sample, and protoplasts were incubated at room temperature for 6–10 h. After treatment with 100 nM flg22 at the indicated time points, protoplasts were collected for co-IP assay in co-IP buffer containing 1% Triton X-100. PYR-41 (Sigma, cat # N2915) was added at the indicated concentrations and time points (see Figure legends).

Recombinant protein isolation and in vitro kinase assays

Fusion proteins were produced from *E. coli* BL21 at 16 °C using LB medium with 0.25 mM isopropyl β-D-1-thiogalactopyranoside (IPTG). GST fusion proteins were purified with Pierce glutathione agarose (Thermo Scientific), and MBP fusion proteins were purified using amylose resin (New England Biolabs) according to the standard protocol from companies. The in vitro kinase assays were performed with 0.5 μg kinase proteins and 5 μg substrate proteins in 30 μl kinase reaction buffer (10 mM Tris-HCl, pH 7.5, 5 mM $MgCl_2$, 2.5 mM EDTA, 50 mM NaCl, 0.5 mM DTT, 50 μM ATP and 1 μCi [γ -^{32}P] ATP). After gentle shaking at room temperature for 2 h, samples were denatured with 4 × SDS loading buffer and separated by 10% SDS–PAGE gel. Phosphorylation was analysed by autoradiography.

In vitro ubiquitination assay

Ubiquitination assays were performed as previously described with modifications[28]. Reactions containing 1 μg substrate, 1 μg HIS_6–E1 (AtUBA1), 1 μg HIS_6–E2 (AtUBC8), 1 μg GST–E3, 1 μg ubiquitin (Boston Biochem, cat # U-100AT-05M) in the ubiquitination reaction buffer (20 mM Tris-HCl, pH 7.5, 5 mM $MgCl_2$, 0.5 mM DTT, 2 mM ATP) were incubated at 30 °C for 3 h. The ubiquitinated proteins were detected by immunoblotting with indicated antibodies. The rabbit monoclonal anti-RHA3A antibody was generated according to the company's standard protocol against the peptide: AGGDSPSPNKGLKKC (GenScript).

In vitro deubiquitination assay

Mouse USP2-cc was cloned by PCR amplification from mouse cDNAs with primers containing BamHI at the 5′ end and SmaI at the 3′ end, followed by BamHI and SmaI digestion and ligation into the *pGST* vector to construct *pGST-Usp2-cc*. GST–USP2-cc fusion proteins were produced in *E. coli* BL21 and purified with Pierce glutathione agarose (Thermo Scientific) according to the manufacturer's standard protocol. Deubiquitination (DUB) assays were performed as previously described with modifications[29]. In brief, an in vitro ubiquitination assay was performed overnight at 28 °C as described above. The reaction was aliquoted into individual tubes containing USP2-cc or heat-inactivated (HI) (95 °C for 5 min) USP2-cc as a control in the DUB reaction buffer (50 mM Tris-HCl, pH 7.5, 50 mM NaCl and 5 mM DTT) and incubated at 28 °C for 5 h. Samples were then denatured and analysed by immunoblotting.

For in vitro DUB assay with flg22-induced ubiquitinated BIK1, BIK1–HA and FLAG–UBQ were expressed in *Arabidopsis* protoplasts treated with 100 nM flg22 for 30 min. The ubiquitinated BIK1–HA proteins were immunoprecipitated as described above. After washing with 50 mM Tris-HCl, agarose beads were washed once with DUB dilution buffer (25 mM Tris-HCl, pH 7.5, 150 mM NaCl and 10 mM DTT) and mixed with GST–USP2-cc in DUB reaction buffer. After overnight incubation, beads were denatured in SDS buffer and analysed by immunoblotting.

MAPK assay

Five 11-day-old *Arabidopsis* seedlings per treatment, grown on vertical plates with ½MS medium, were transferred into water overnight before flg22 treatment. Seedlings were collected, drilled and lysed in 100 μl co-IP buffer. Protein samples with 1 × SDS buffer were separated in 10%

SDS–PAGE gel to detect pMPK3, pMPK6 and pMPK4 by immunoblotting with anti-pERK1/2 antibody (Cell Signaling, cat # 9101).

Detection of ROS production

The third or fourth pair of true leaves from 4- to 5-week-old soil-grown *Arabidopsis* plants were punched into leaf discs (diameter 5 mm). Leaf discs were incubated in 100 µl ddH_2O with gentle shaking overnight. Water was replaced with 100 µl reaction solution containing 50 µM luminol, 10 µg/ml horseradish peroxidase (Sigma-Aldrich) supplemented with or without 100 nM flg22. Luminescence was measured with a luminometer (GloMax-Multi Detection System, Promega) with a setting of 1 min as the interval for 40–60 min. Detected values of ROS production were indicated as means of relative light units (RLU).

In vitro GST pull-down assay

GST or GST–BIK1 agarose beads were obtained after elution and washed with 1× PBS (137 mM NaCl, 2.7 mM KCl, 15 mM Na_2HPO_4, 4.4 mM KH_2PO_4) three times. HA-tagged MBP-$RHA3A^{CD}$ or MBP proteins (2 µg) were pre-incubated with 10 µl prewashed glutathione agarose beads in 300 µl pull-down incubation buffer (20 mM Tris-HCl, pH 7.5, 100 mM NaCl, 0.1 mM EDTA, and 0.2% Triton X-100) for 30 min at 4 °C. Five microlitres of GST or GST–BIK1 agarose beads were pre-incubated with 20 µg bovin serum albumin (BSA, Sigma, cat # A7906) in 300 µl incubation buffer for 30 min at 4 °C with gentle shaking. The supernatant containing MBP-$RHA3A^{CD}$ or MBP was incubated with pre-incubated GST or GST–BIK1 agarose beads for 1 h at 4 °C with gentle shaking. The agarose beads were precipitated and washed three times in pull-down wash buffer (20 mM Tris-HCl, pH 7.5, 300 mM NaCl, 0.1 mM EDTA, and 0.5% Triton X-100). The pulled-down proteins were analysed by immunoblotting with an anti-MBP antibody (Biolegend, cat # 906901).

Mass spectrometry analysis of ubiquitination sites

In vitro ubiquitination reactions with GST–$RHA3A^{CD}$ and GST–BIK1 or GST–BIK1(K204R) were performed as mentioned above with overnight incubation. Reactions were loaded on an SDS–PAGE gel (7.5%) and ran for a relatively short time until the ubiquitinated bands could be separated from the original GST–BIK1 (GST–BIK1 band ran less than 0.5 cm from the separating gel). Ubiquitinated bands were sliced and trypsin-digested before LC–MS/MS analysis on an LTQ-Orbitrap hybrid mass spectrometer (Thermo Fisher) as previously described[30]. The MS/MS spectra were analysed with SEQUEST software, and images were exported from SEQUEST.

In vivo BIK1 ubiquitination sites were identified as follows: 20 ml of wild-type *Arabidopsis* protoplasts at a concentration of 2×10^5 per ml were transfected with BIK1–GFP and FLAG–UBQ and the protoplasts were treated with 200 nM flg22 for 30 min after 7 h of incubation. GFP-trap-Agarose beads (Chromotek, cat # gta-20) were incubated with cell lysates at a ratio of 10 µl beads to 4×10^5 cells for 1 h at 4 °C and beads were pooled from 10 tubes, washed using IP buffer three times, and denatured in SDS buffer. Samples were separated by 10% SDS–PAGE and stained with GelCode Blue Stain Reagent (Thermo Fisher cat # 24590). Ubiquitinated bands were sliced and analysed as described above.

Confocal microscopy and image analysis

For laser scanning confocal microscopy, images were taken using a Leica SP8X inverted confocal microscope equipped with a HC PL APO CS2 40×/1.10 and 63×/1.20 water-corrected objective. The excitation wavelength was 488 nm for both GFP and FM4-64 (Thermo Fisher T13320), 514 nm for YFP and 555 nm for TagRFP using the white light laser. Emission was detected at 500–530 nm for GFP, 570–670 nm for FM4-64, 519–549 nm for YFP, and 569–635 nm for TagRFP by using Leica hybrid detectors. Autofluorescence was removed by adjusting the time gate window between 0.8 and 6 ns. Intensities were manipulated using ImageJ software.

For SDCM, image series were captured using a custom Olympus IX-71 inverted microscope equipped with a Yokogawa CSU-X1 5,000 rpm spinning disc unit and 60× silicon oil objective (Olympus UPlanSApo 60×/1.30 Sil) as previously described[11]. For the custom SDCM system, GFP and FM4-64 were excited with a 488-nm diode laser and fluorescence was collected through a series of Semrock Brightline 488-nm single-edge dichroic beamsplitter and bandpass filters: 500–550 nm for GFP and 590–625 nm for FM4-64. Camera exposure time was set to 150 ms. For each image series, 67 consecutive images at a *z*-step interval of 0.3 µm (20 µm total depth) were captured using Andor iQ2 software (Belfast, UK). Images captured by custom SDCM were processed with the Fiji distribution of ImageJ 1.51 (https://fiji.sc/) software, and BIK1–GFP and FLS2–GFP endosomal puncta were quantified as the number of puncta per 1,000 μm^2 as previously described[11,31], with the exception that puncta were detected within a size distribution of 0.1–2.5 μm^2. For colocalization of BIK1–GFP with FM4-64 by custom SDCM, cotyledons were stained with 2.5 µM FM4-64 for 10 min, washed twice, and imaged after a 5-min chase.

For quantification of flg22-induced puncta containing BIK1–GFP or BIK1(9KR)-GFP over time, the maximum number of FM4-64 labelled spots per image area was set to 100%, and the percentage of GFP-colocalizing spots per time interval relative to the maximum was calculated; 20–25 images per time interval, captured from 5 individual plants per genotype were used for quantification.

For transient expression in *N. benthamiana, Agrobacterium* strain C58 carrying the constructs of interest was co-infiltrated in the abaxial side of tobacco leaves as described previously[32]. Between 48 and 72 h after infiltration, multiple infiltrated leaves were treated with 100 µM flg22 and imaged at the indicated time points. The number of puncta per 1,000 μm^2 was quantified as previously described[11,31]. The percentage colocalization of BIK1 and FLS2 was calculated by dividing the number of BIK1–FLS2 colocalizing puncta by the total number of BIK1 puncta. The percentage colocalization of BIK1 and ARA6 was calculated by dividing the number of BIK1–ARA6 or BIK1(9KR)–ARA6 colocalizing puncta by the total number of ARA6 puncta.

qRT–PCR analysis

Total RNA was isolated from the leaves of four-week-old plants with TRIzol reagent (Invitrogen). One microgram of total RNA was treated with RNase-free DNase I (New England Biolabs) followed by cDNA synthesis with M-MuLV reverse transcriptase (New England Biolabs) and oligo(dT) primer. qRT–PCR analysis was performed using iTaq SYBR green Supermix (Bio-Rad) with primers listed in Supplementary Table 1 in a Bio-Rad CFX384 Real-Time PCR System. The expression of *RHA3A* and *RHA3B* was normalized to the expression of *ACTIN2*.

Reporting summary

Further information on research design is available in the Nature Research Reporting Summary linked to this paper.

Data availability

The data supporting the findings of this study are available within the paper and its Supplementary Information files. Source Data (gels and graphs) for Figs. 1–4 and Extended Data Figs. 1–10 are provided with the paper.

25. Wang, Z. P. et al. Egg cell-specific promoter-controlled CRISPR/Cas9 efficiently generates homozygous mutants for multiple target genes in *Arabidopsis* in a single generation. *Genome Biol*. **16**, 144 (2015).
26. Tao, K., Waletich, J. R., Arredondo, F. & Tyler, B. M. Manipulating endoplasmic reticulum-plasma membrane tethering in plants through fluorescent protein complementation. *Front. Plant Sci*. **10**, 635 (2019).
27. He, P., Shan, L. & Sheen, J. The use of protoplasts to study innate immune responses. *Methods Mol. Biol*. **354**, 1–9 (2007).
28. Zhou, J., He, P. & Shan, L. Ubiquitination of plant immune receptors. *Methods Mol. Biol*. **1209**, 219–231 (2014).

29. Hospenthal, M. K., Mevissen, T. E. T. & Komander, D. Deubiquitinase-based analysis of ubiquitin chain architecture using Ubiquitin Chain Restriction (UbiCRest). *Nat. Protocols* **10**, 349–361 (2015).
30. Xu, P. et al. Quantitative proteomics reveals the function of unconventional ubiquitin chains in proteasomal degradation. *Cell* **137**, 133–145 (2009).
31. Leslie, M. E. & Heese, A. Quantitative analysis of ligand-induced endocytosis of FLAGELLIN-SENSING 2 using automated image segmentation. *Methods Mol. Biol*. **1578**, 39–54 (2017).
32. Boruc, J. et al. Functional modules in the *Arabidopsis* core cell cycle binary protein-protein interaction network. *Plant Cell* **22**, 1264–1280 (2010).

Acknowledgements We thank Q. Chen for the CRISPR–Cas9 system, J. Li and J. Sheen for the amiRNA system, P. de Figueiredo for mouse cDNA, and T. Devarenne, M. Dickman, C. Kaplan, T. Igumenova, J. Sheen, and the members of the Shan and He laboratories for discussion and comments on this work. The work was supported by NIH (R01GM097247) and the Robert A. Welch foundation (A-1795) to L.S., National Science Foundation (NSF) (MCB-1906060) and NIH (R01GM092893) to P.H., NSF (IOS-1147032) to A.H., the Special Research Fund (BOF15/24J/048) to E.R., and NIH (R01GM114260) to J.P.

Author contributions X.M., P.H. and L.S. conceived and designed the experiments; X.M. performed most of the molecular, biochemical and transgenic experiments; L.A.N.C. and D.V.S., under the supervision of E.R., conducted BIK1, BIK1(9KR) and FLS2 endocytosis experiments in the transgenic plants and *N. benthamiana*, colocalization with ARA6, and spatial and temporal dynamics of BIK1 and FLS2 endocytosis in *N. benthamiana;* M.E.L., under the supervision of A.H., performed BIK1 and FLS2 endocytosis in transgenic plants by spinning disc confocal microscopy; K.T., under the supervision of B.M.T., conducted BIK1(G2A) localization, BIK1 endocytosis and colocalization with ARA6 experiments in *N. benthamiana;* Z.W., under the supervision of J.P., identified BIK1 in vivo and in vitro ubiquitination sites with LC–MS/MS; J.L. performed co-IP and *Botrytis* infection assays; X.Y. performed co-IP and transgenic plant assays; B.L. generated *35S::BIK1-GFP* transgenic plants; J.Z. performed in vitro kinase assays; E.R., A.H., B.T., and J.P. analysed data, provided critical feedback and helped to shape the research. All experiments were independently reproduced in different laboratories. X.M., P.H. and L.S. wrote the manuscript with input from all authors.

Competing interests The authors declare no competing interests.

Additional information

Supplementary information is available for this paper at https://doi.org/10.1038/s41586-020-2210-3.

Correspondence and requests for materials should be addressed to P.H. or L.S.

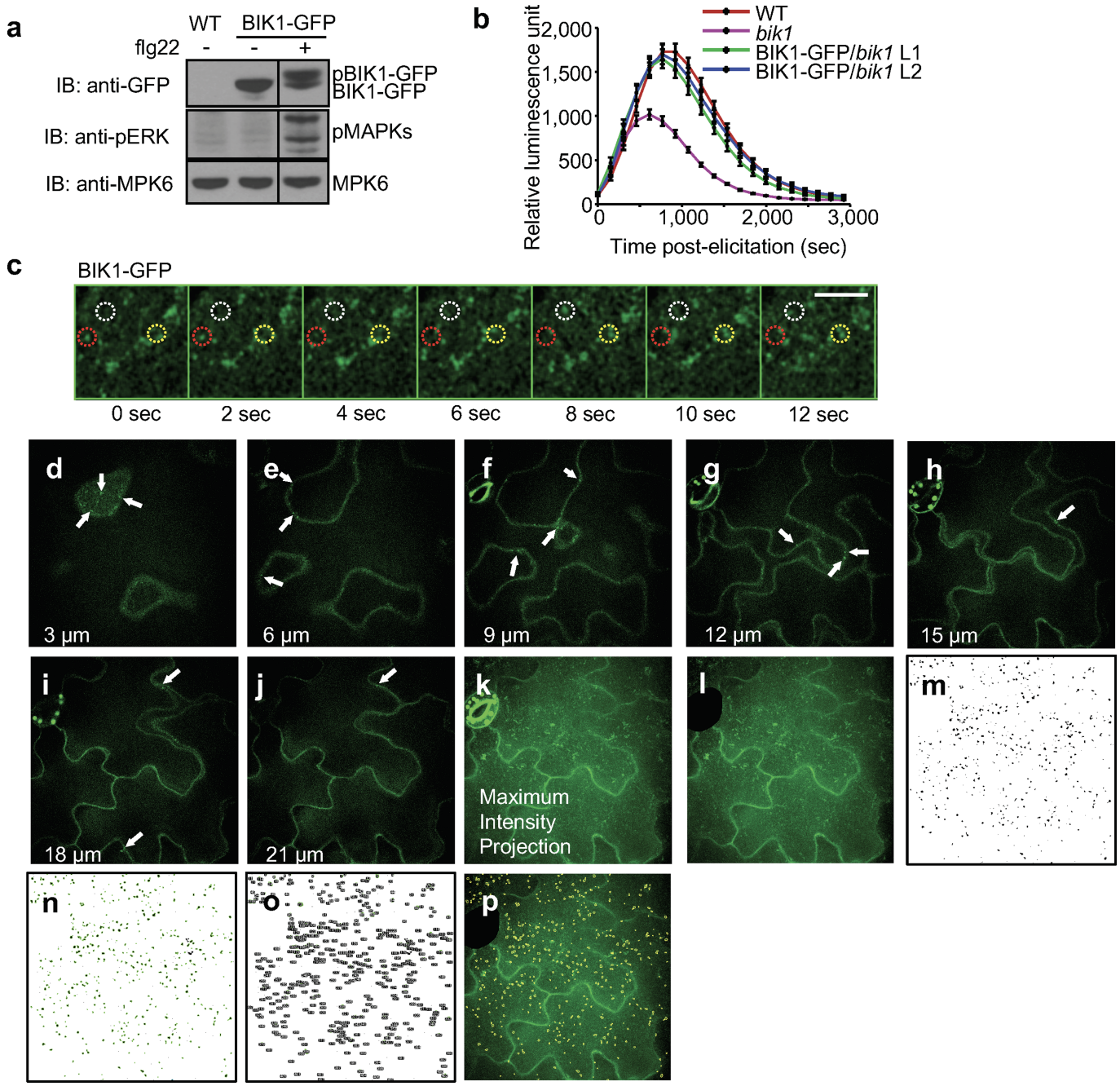

Extended Data Fig. 1 | BIK1–GFP is functional in plants and undergoes endocytosis. a, BIK1–GFP is functional, as confirmed by BIK1 phosphorylation in *35S::BIK1-GFP*-expressing Col-0 cotyledons after treatment with 1 µM flg22. MPK6 is a loading control and the black stippled line indicates discontinuous segments from the same gel. **b**, BIK1–GFP restored ROS production in *bik1* leaves upon flg22 treatment. Leaf discs from wild-type, *bik1* and BIK1–GFP complementation plants (lines 1 and 2) were treated with 100 nM flg22 for ROS measurement using a luminometer over 50 min. Data are shown as mean ± s.e.m. (wild-type, *bik1*: $n = 42$; BIK1–GFP/*bik1*: $n = 45$). **c**, Time-lapse SDCM shows that BIK1–GFP endosomal puncta are highly mobile with puncta that disappear (red circle), appear (yellow circle), and rapidly move in and out of the plane of view (white circle). Scale bar, 5 µm. **d**–**k**, BIK1–GFP localizes to endosomal puncta and plasma membrane in cross-sectional images of epidermal cells. The abaxial epidermal cells of cotyledons expressing BIK1–GFP were imaged with SDCM with a *Z*-step of 0.3 µm. A subset of the cross-sectional images is shown at the indicated depths (3, 6, 9, 12, 15, 18 and 21 µm) along with the maximum-intensity projection (MIP) of all 67 images through the epidermis. BIK1–GFP localizes to both plasma membrane and endosomal puncta (white arrows) within all sections. **k**–**p**, Method for quantification of BIK1–GFP puncta within MIPs of SDCM images. **k**, MIPs were generated using Fiji distribution of ImageJ 1.51 (https://fiji.sc/) for each *Z*-series captured by SDCM imaging of BIK1–GFP cotyledons. **l**, Regions of MIP with non-pavement cells (for example, stomata) were removed from the image using the line draw and crop functions. The total surface area (µm^2) of the image was measured using the analyze measure function. **m**, Puncta within the cropped MIP were recognized using a customized model generated and applied with the Trainable Weka Segmentation plug-in for Fiji. The same model was applied to all images to generate binary images showing the physical locations of all BIK1–GFP puncta (black). **n**–**o**, Puncta within the size range 0.1–2.5 µm^2 were highlighted in green (**n**) and counted (**o**) using the analyze particles function in Fiji. BIK1–GFP endocytosis was quantified as the number of puncta per 1,000 µm^2. **p**, An overlay of the BIK1–GFP puncta (yellow highlight) over the cropped MIP confirmed correct identification of puncta. The experiments in **a**–**c** were repeated three times with similar results.

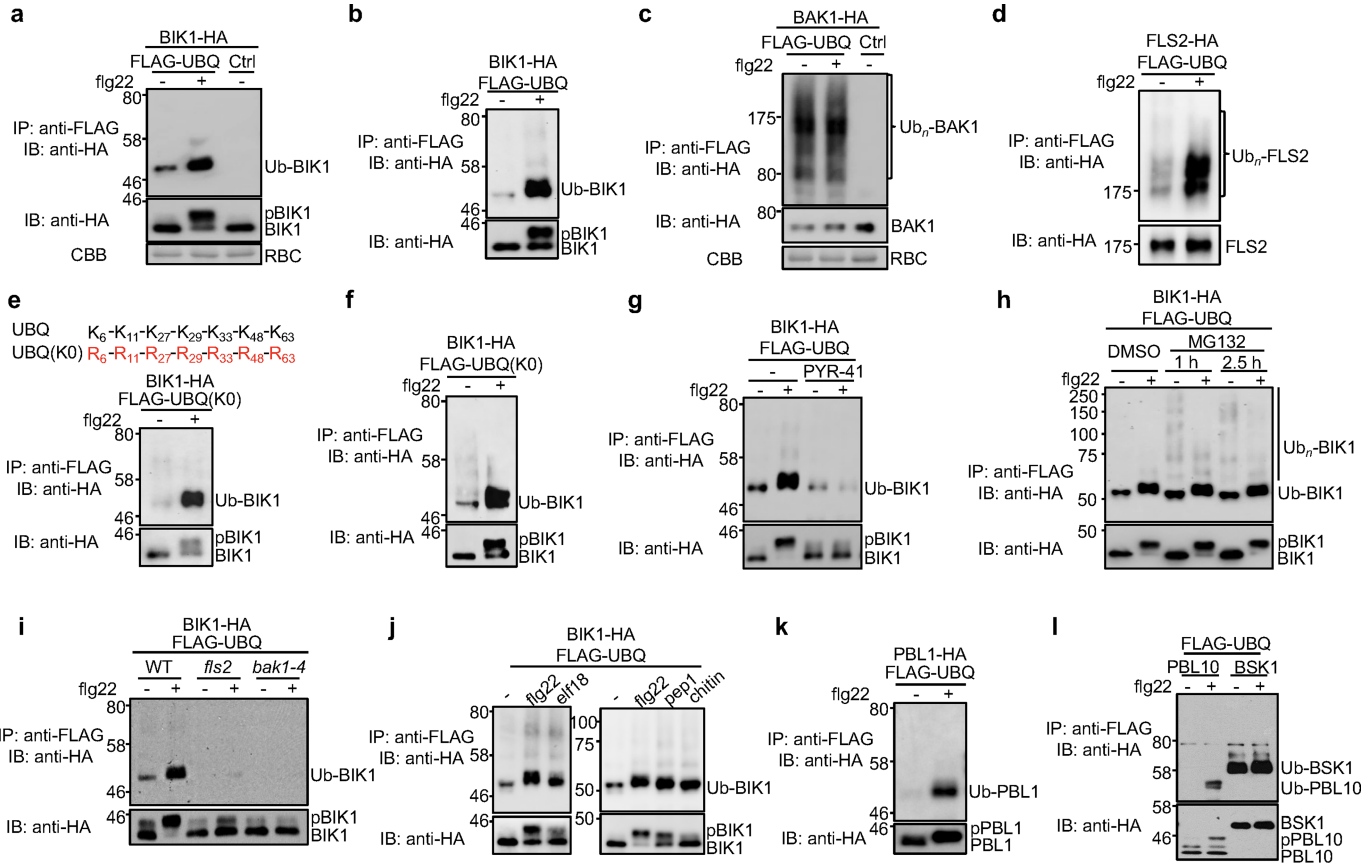

Extended Data Fig. 2 | MAMP-triggered monoubiquitination of BIK1-family RLCK proteins. a, Flg22 induces monoubiquitination of BIK1. Protoplasts from wild-type plants were transfected with BIK1–HA and FLAG–UBQ or a vector (Ctrl), and then treated with 100 nM flg22 for 30 min. After immunoprecipitation with anti-FLAG agarose, ubiquitinated BIK1 was detected by immunoblotting using anti-HA antibody (top). Middle, BIK1–HA proteins; bottom, CBB staining for RuBisCO (RBC). **b**, Flg22 induces BIK1 monoubiquitination in *pBIK1::BIK1-HA* transgenic plants. Protoplasts from *pBIK1::BIK1-HA/bik1* transgenic plants were transfected with FLAG–UBQ and then treated with 100 nM flg22 for 30 min. After immunoprecipitation with anti-FLAG agarose, ubiquitinated BIK1 was detected by immunoblotting with anti-HA antibody (top). Bottom, BIK1–HA proteins. **c**, BAK1 is constitutively polyubiquitinated in vivo. Protoplasts from wild-type plants were transfected with BAK1–HA and FLAG–UBQ or control, and then treated with 100 nM flg22 for 30 min. Immunoprecipitation was carried out with anti-FLAG agarose. Ub$_n$-BAK1 proteins were detected as a smear with anti-HA immunoblotting (top). Middle, BAK1–HA proteins; bottom, CBB staining for RBC. **d**, Flg22 induces FLS2 polyubiquitination. Protoplasts from wild-type plants were transfected with FLS2–HA and FLAG–UBQ and then treated with 100 nM flg22 for 30 min. **e**, **f**, Monoubiquitination of BIK1 with UBQ(K0). Protoplasts from *pBIK1::BIK1-HA* (**e**) or *35S::BIK1-HA* (**f**) transgenic plants were transfected with FLAG–UBQ(K0) (all lysine residues mutated to arginine) and then treated with 100 nM flg22 for 30 min. The mutations of lysine to arginine in UBQ(K0) are shown at the top of **e** with amino-acid positions labelled. **g**, PYR-41 blocks flg22-induced BIK1 monoubiquitination. PYR-41 (50 μM) was added 30 min before flg22 treatment. **h**, Flg22 induces BIK1 monoubiquitination in the presence of MG132. MG132 (2 μM) was added 1 h or 2.5 h before treatment with flg22. **i**, Flg22-induced BIK1 monoubiquitination depends on FLS2 and BAK1. Protoplasts isolated from wild-type, *fls2* or *bak1-4* plants were transfected with BIK1–HA and FLAG–UBQ and then treated with 100 nM flg22 for 30 min. **j**, elf18, pep1 and chitin induce BIK1 monoubiquitination. 1 μM elf18, 200 nM pep1 or 100 μg/ml chitin was added to protoplasts for 30 min. **k**, The BIK1 homologue PBL1 is monoubiquitinated upon treatment with flg22. PBL1–HA and FLAG–UBQ were expressed in protoplasts. **l**, Flg22 induces monoubiquitination of the BIK1-family RLCK PBL10 but not of BSK1. HA-tagged PBL10 or BSK1 was expressed with FLAG–UBQ in wild-type protoplasts. Experiments were repeated at least three times with similar results.

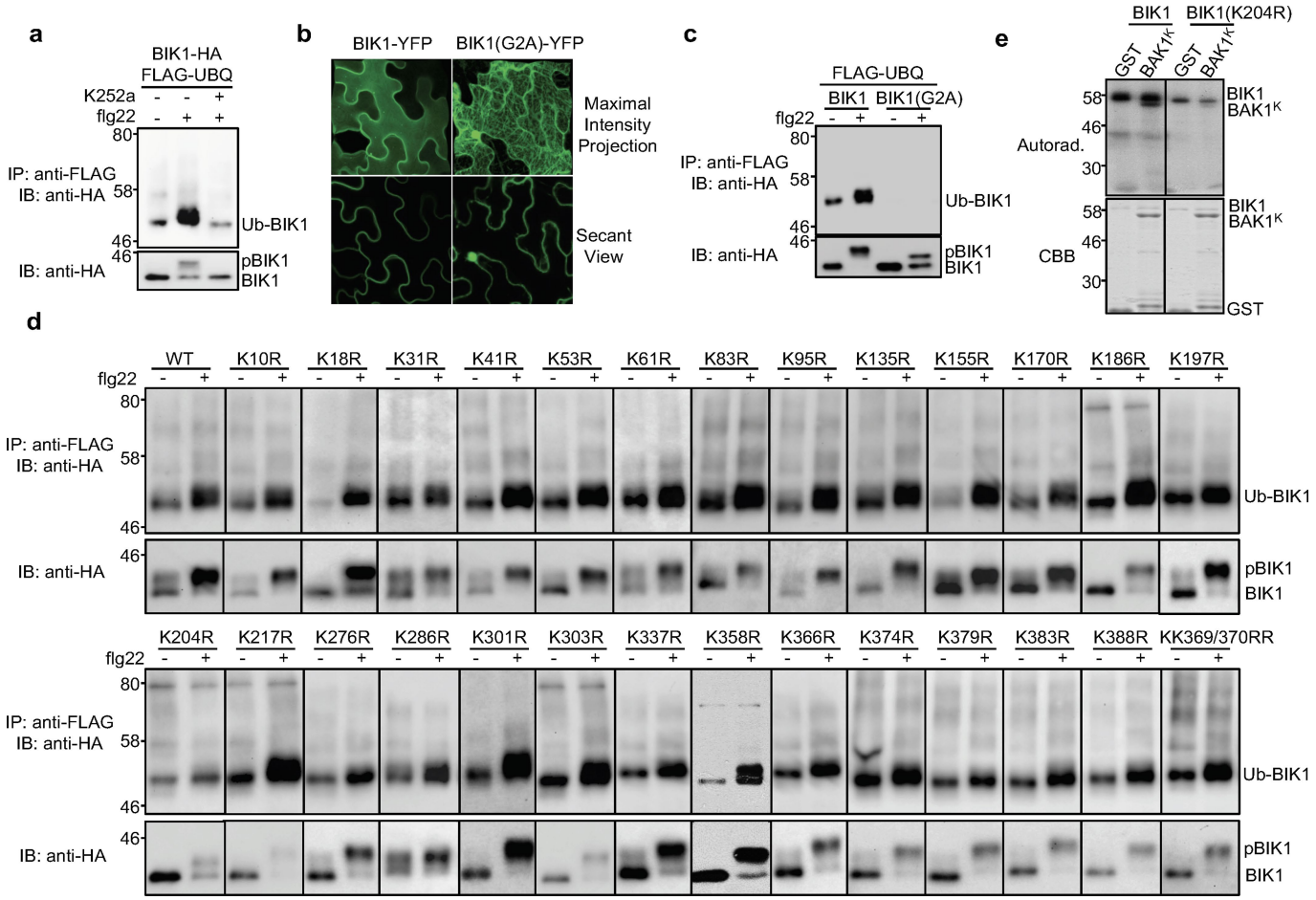

Extended Data Fig. 3 | Plasma membrane localization and phosphorylation are required for BIK1 ubiquitination. a, The kinase inhibitor K252a blocks flg22-induced ubiquitination of BIK1. Protoplasts transfected with FLAG–UBQ and BIK1–HA were treated with 1 μM K252a for 30 min and then with 100 nM flg22. **b**, BIK1(G2A) no longer localizes to the plasma membrane. BIK1–YFP or BIK1(G2A)–YFP was expressed in *N. benthamiana* for imaging analysis. **c**, BIK1(G2A) show compromised flg22-induced monoubiquitination. BIK1–HA or BIK1(G2A)–HA was co-expressed with FLAG–UBQ in protoplasts. **d**, Single K-to-R mutations of BIK1 fail to block flg22-induced ubiquitination without altering kinase activity. HA-tagged wild-type or mutant BIK1 was co-expressed with FLAG–UBQ in protoplasts. **e**, BIK1(K204R) exhibits reduced autophosphorylation and phosphorylation of BAK1. An in vitro kinase assay was performed using GST–BIK1 or GST–BIK1(K204R) as a kinase and GST or GST–$BAK1^{K}$ ($BAK1^{K}$ kinase domain without detectable autophosphorylation activity) as a substrate with [γ-^{32}P] ATP. Top, proteins were separated with SDS–PAGE and analysed by autoradiography (Autorad.); bottom, protein loading shown CBB staining. Experiments were repeated at least twice with similar results.

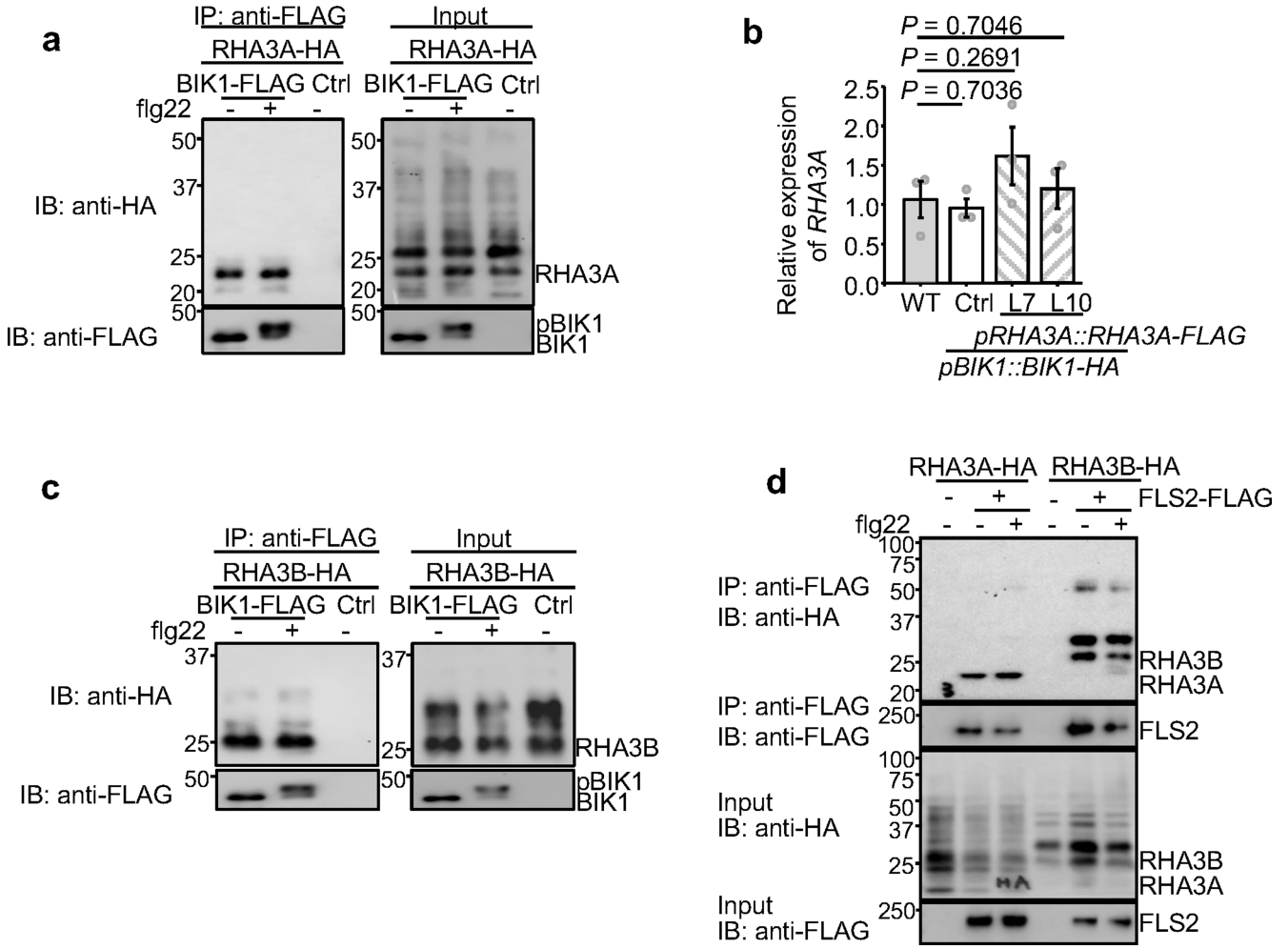

Extended Data Fig. 4 | RHA3A/B interacts with BIK1 in vivo. a, BIK1 interacts with RHA3A in a co-IP assay. RHA3A–HA was co-expressed with BIK1–FLAG or control in protoplasts and then treated with 100 nM flg22 for 15 min. Left, the co-IP assay was carried out with anti-FLAG agarose and immunoprecipitated proteins were immunoblotted with anti-HA or anti-FLAG antibody. Right, BIK1–FLAG and RHA3A–HA proteins. **b**, *RHA3A* expression (mean ± s.e.m.) in *pRHA3A::RHA3A-FLAG/pBIK1::BIK1-HA* transgenic plants. qRT–PCR was carried out to detect *RHA3A* transcripts using *ACTIN2* as a control. Relative gene expression in wild-type (set as 1), *pBIK1::BIK1-HA* (Ctrl) and two independent transgenic lines (lines 7 and 10) is shown. One-way ANOVA, $n = 3$. **c**, BIK1 associates with RHA3B independent of flg22 treatment. RHA3B–HA was co-expressed with BIK1–FLAG or control in protoplasts and then treated with 100 nM flg22 for 15 min. Left, co-IP assay was carried out with anti-FLAG agarose and immunoprecipitated proteins were immunoblotted with anti-HA or anti-FLAG antibody. Right, BIK1–FLAG and RHA3B–HA proteins before immunoprecipitation. **d**, FLS2 interacts with RHA3A and RHA3B in a co-IP assay. Experiments were repeated three times with similar results.

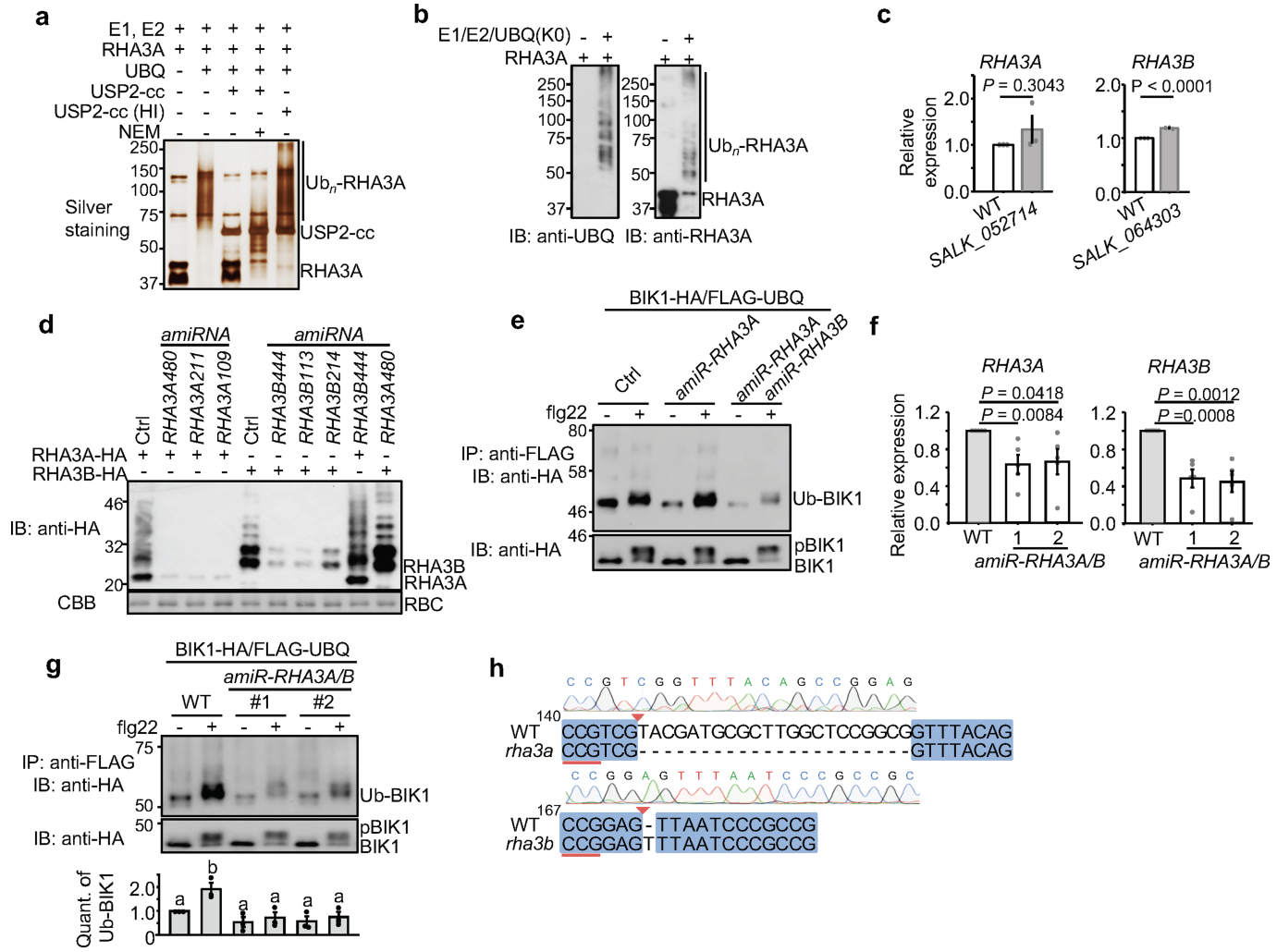

Extended Data Fig. 5 | RHA3A/B ubiquitinate BIK1 in vivo. a, GST–RHA3A^{CD} possesses E3 ligase activity in vitro. An in vitro ubiquitination assay was performed with GST–RHA3A^{CD} followed by deubiquitination reactions with GST–USP2-cc. *N*-ethylmaleimide (NEM) (10 mM), an inhibitor of deubiquitinases, and heat-inactivated (HI, 95 °C for 5 min) USP2-cc are controls. Samples were analysed by SDS–PAGE and silver staining. **b**, GST–RHA3A^{CD} possesses multi-monoubiquitination activity in vitro. A ubiquitination assay was done as in **a** but using the ubiquitin mutant with all lysine residues mutated to arginine (UBQ(K0)). Ubiquitinated proteins were detected by immunoblotting with anti-UBQ (left) or anti-RHA3A (right) antibodies. **c**, *RHA3* expression in T-DNA insertion mutants. *RHA3A* expression in the T-DNA knockout line *SALK_052714* and *RHA3B* expression in *SALK_064303* were analysed as in Extended Data Fig. 4b. Mean ± s.e.m. fold change (WT set as 1.0); two-tailed Student's *t*-test, $n = 3$. **d**, Screen for the optimal *amiR-RHA3A* and *amiR-RHA3B*. Protoplasts were transfected with *RHA3A-HA* or *RHA3B-HA* with control, *amiR-RHA3A* or *amiR-RHA3B*. RHA3A or RHA3B proteins were examined by immunoblotting with anti-HA antibody. **e**, RHA3A and RHA3B are required for BIK1 ubiquitination in vivo. A BIK1 ubiquitination assay was carried out by co-expressing control, artificial microRNA targeting *RHA3A* (*amiR-RHA3A*) or *amiR-RHA3A* together with microRNA targeting *RHA3B* (*amiR-RHA3A amiR-RHA3B*). **f**, *RHA3A* and *RHA3B* expression in *amiR-RHA3A/B* transgenic plants. qRT–PCR was carried out to detect *RHA3A* and *RHA3B* transcripts with *ACTIN2* as a control. Mean ± s.e.m. fold change in gene expression from two independent transgenic lines (lines 1 and 2); one-way ANOVA, $n = 5$. **g**, RHA3A and RHA3B are required for BIK1 ubiquitination in transgenic plants. Protoplasts from *amiR-RHA3A/B* transgenic plants were transfected with BIK1–HA and FLAG–UBQ for ubiquitination assay. Bottom, quantification of BIK1 ubiquitination in *amiR-RHA3A/B* transgenic plants. Intensity of Ub-BIK1 or BIK1 bands was quantified with Image Lab (Bio-Rad). The amount of BIK1 ubiquitination is the relative intensity of the Ub-BIK1 band to the BIK1 band (no treatment in wild-type set as 1.0). Mean ± s.e.m.; different letters indicate significant difference with others ($P < 0.05$, one-way ANOVA, $n = 3$). **h**, Sequencing analysis of *RHA3A* and *RHA3B* genes in the CRISPR–Cas9 *rha3a/b* mutant. PCR fragments corresponding to *RHA3A* and *RHA3B* in *rha3a/b* were amplified, sequenced, and aligned to wild-type coding sequences. The reverse complement of the PAM sequence is underlined in red, and red arrowheads indicate the theoretical Cas9 cleavage sites. The experiments were repeated three times with similar results.

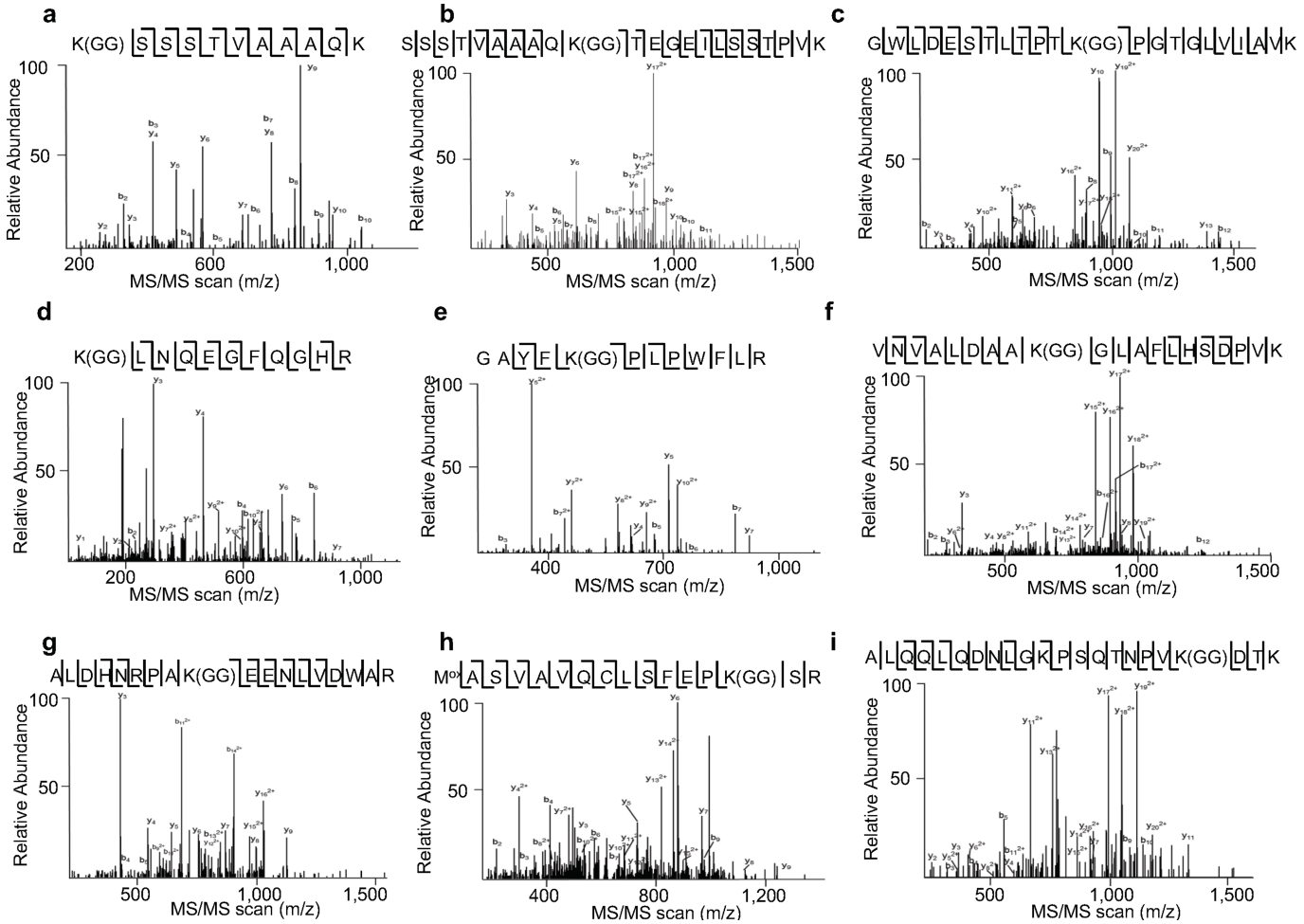

Extended Data Fig. 6 | BIK1 in vitro ubiquitination sites identified by mass spectrometry. MS/MS spectra of peptides containing ubiquitinated lysine residues of BIK1. **a**, K31; **b**, K41; **c**, K95; **d**, K106; **e**, K170; **f**, K186; **g**, K286; **h**, K337; **I**, K366. MS spectra are outputs from the SEQUEST program. MS analysis was performed once.

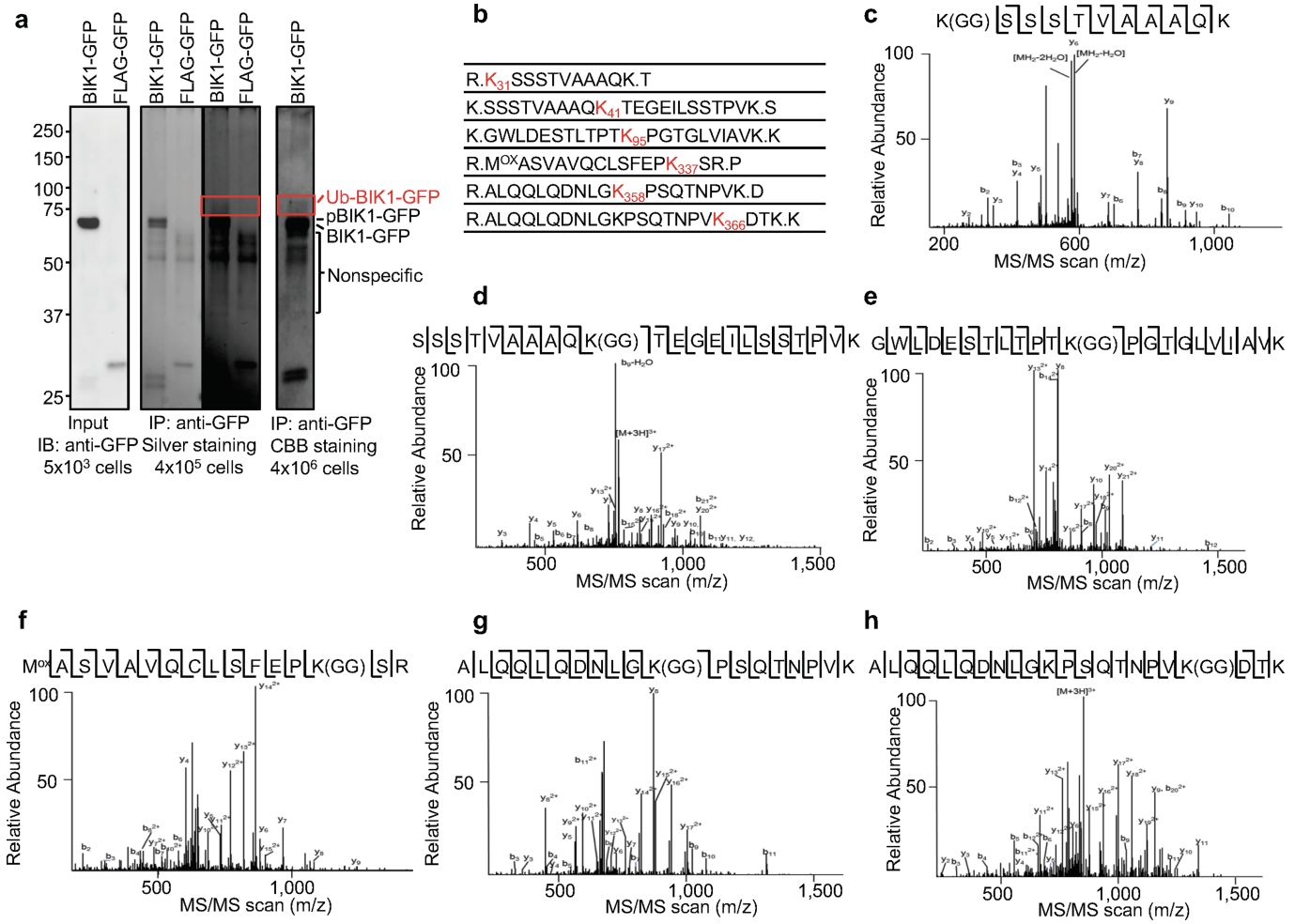

Extended Data Fig. 7 | BIK1 in vivo ubiquitination sites identified by mass spectrometry. a, Ubiquitinated BIK1–GFP in planta was immunoprecipitated for LC–MS/MS analysis. BIK1–GFP and FLAG–UBQ were co-expressed in wild-type protoplasts (about 4×10^6 cells) and then treated with 200 nM flg22 for 30 min. Ubiquitinated BIK1 was immunoprecipitated with GFP-trap-agarose, separated by SDS–PAGE, digested with trypsin and subjected to LC–MS/MS analysis. Portions of cell lysates were examined for BIK1–GFP expression (left), and immunoprecipitates were analysed by SDS–PAGE following silver staining (middle; right for longer exposure of the same gel) and SDS–PAGE following CBB staining (right). The highlighted area was cut and analysed by MS. **b**, BIK1 is ubiquitinated in vivo. Ubiquitinated lysines containing a diglycine remnant identified by LC–MS/MS analysis are marked in red with amino acid positions. **c**–**h**, MS/MS spectra of peptides containing ubiquitinated lysines of BIK1 are shown. **c**, K31; **d**, K41; **e**, K95; **f**, K337; **g**, K358; **h**, K366. MS spectra are outputs from the SEQUEST program. MS analysis was performed once.

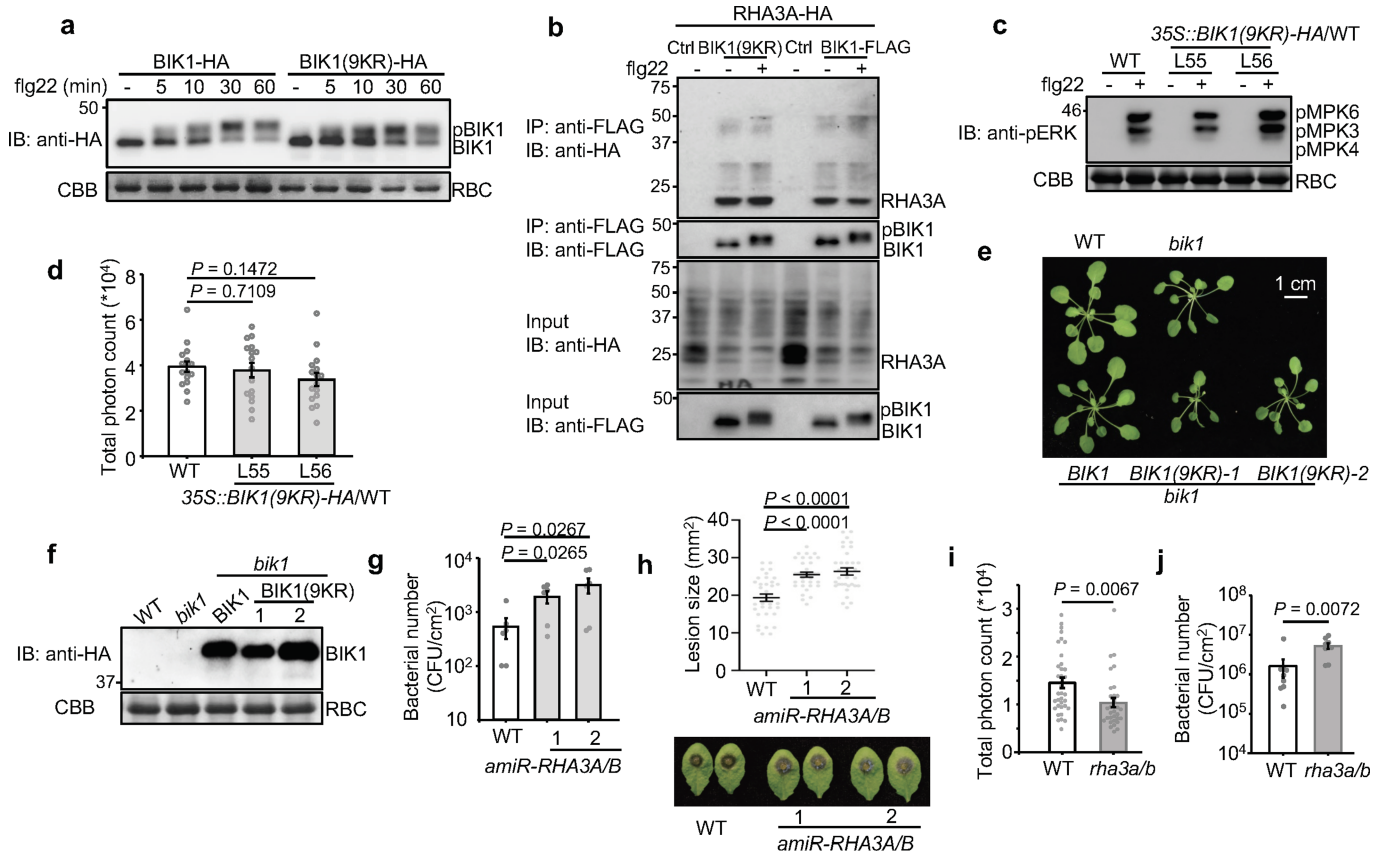

Extended Data Fig. 8 | BIK1 monoubiquitination is required for plant defence and flg22 signalling. a, BIK1(9KR) undergoes phosphorylation similar to BIK1 upon flg22 treatment. BIK1–HA or BIK1(9KR)–HA was expressed in wild-type protoplasts which were then treated with 100 nM flg22 for the indicated times. Band-shift of BIK1 was examined by immunoblotting with anti-HA antibody. **b**, BIK1(9KR) interacts with RHA3A in a co-IP assay. RHA3A–HA was co-expressed with BIK1–FLAG or BIK1(9KR)–FLAG in protoplasts that were then treated with 100 nM flg22 for 15 min. Co-IP assay was carried out with anti-FLAG agarose and immunoprecipitated proteins were immunoblotted with anti-HA or anti-FLAG antibody (top two panels). Bottom two panels show BIK1–FLAG or BIK1(9KR)–FLAG and RHA3A–HA proteins. **c**, Transgenic plants with *BIK1*^{9KR} overexpression in wild-type background show similar MAPK activation to wild-type plants. Eleven-day-old seedlings of wild-type or *35S::BIK1*^{9KR}*-HA*/WT transgenic plants (lines 55 and 56) were treated with 200 nM flg22 for 15 min. MAPK activation was analysed with anti-pERK antibody (top), and protein loading is shown by CBB staining for RBC (bottom). **d**, Transgenic plants with *BIK1*^{9KR} overexpression in wild-type background show similar flg22-induced ROS production to wild-type plants. Leaf discs from the indicated genotypes were treated with 100 nM flg22, and ROS production was measured as relative luminescence units by a luminometer over 50 min. Mean total photon count ± s.e.m. overlaid with dot plot (one-way ANOVA, $n = 16$). **e**, Growth phenotype of *pBIK1::BIK1-HA/bik1* and *pBIK1::BIK1*^{9KR}*-HA/bik1* transgenic plants. Five-week-old soil-grown plants are shown. Scale bar, 1 cm. **f**, Expression of BIK1–HA or BIK1(9KR)–HA in transgenic plants. Top, total proteins from leaves of four-week-old transgenic plants were subjected to anti-HA immunoblotting. Bottom, CBB staining for RBC. **g**, RHA3A and RHA3B are involved in resistance to *Pst* DC3000 *hrcC*$^-$ infection. Plants were spray-inoculated with *Pst* DC3000 *hrcC*$^-$ and bacterial growth was measured at 4 dpi. Mean ± s.e.m. overlaid with dot plots (one-way ANOVA, $n = 6$). **h**, RHA3A and RHA3B are involved in resistance to *Botrytis*. Four-week-old plant leaves were deposited with 10 µl *B. cinerea* BO5 at a concentration of 2.5×10^5 spores per ml. Disease symptoms were recorded, and the lesion diameter was measured at 2 dpi. Mean ± s.e.m. overlaid with dot plots (one-way ANOVA, $n = 34$). **i**, ROS production is reduced in *rha3a/b* plants. Leaf discs from wild-type or *rha3a/b* plants were treated with 100 nM flg22 and ROS production measured over 50 min. Mean ± s.e.m. total photon count overlaid with dot plots (two-tailed Student's *t*-test, $n = 36$ for wild-type and $n = 32$ for *rha3a/b*). **j**, RHA3A and RHA3B are involved in resistance to *Pst* DC3000. Plants were spray-inoculated with *Pst* DC3000 and bacterial growth was measured at 3 dpi. Mean ± s.e.m. overlaid with dot plots (two-tailed Student's *t*-test, $n = 9$). Experiments were repeated three times with similar results.

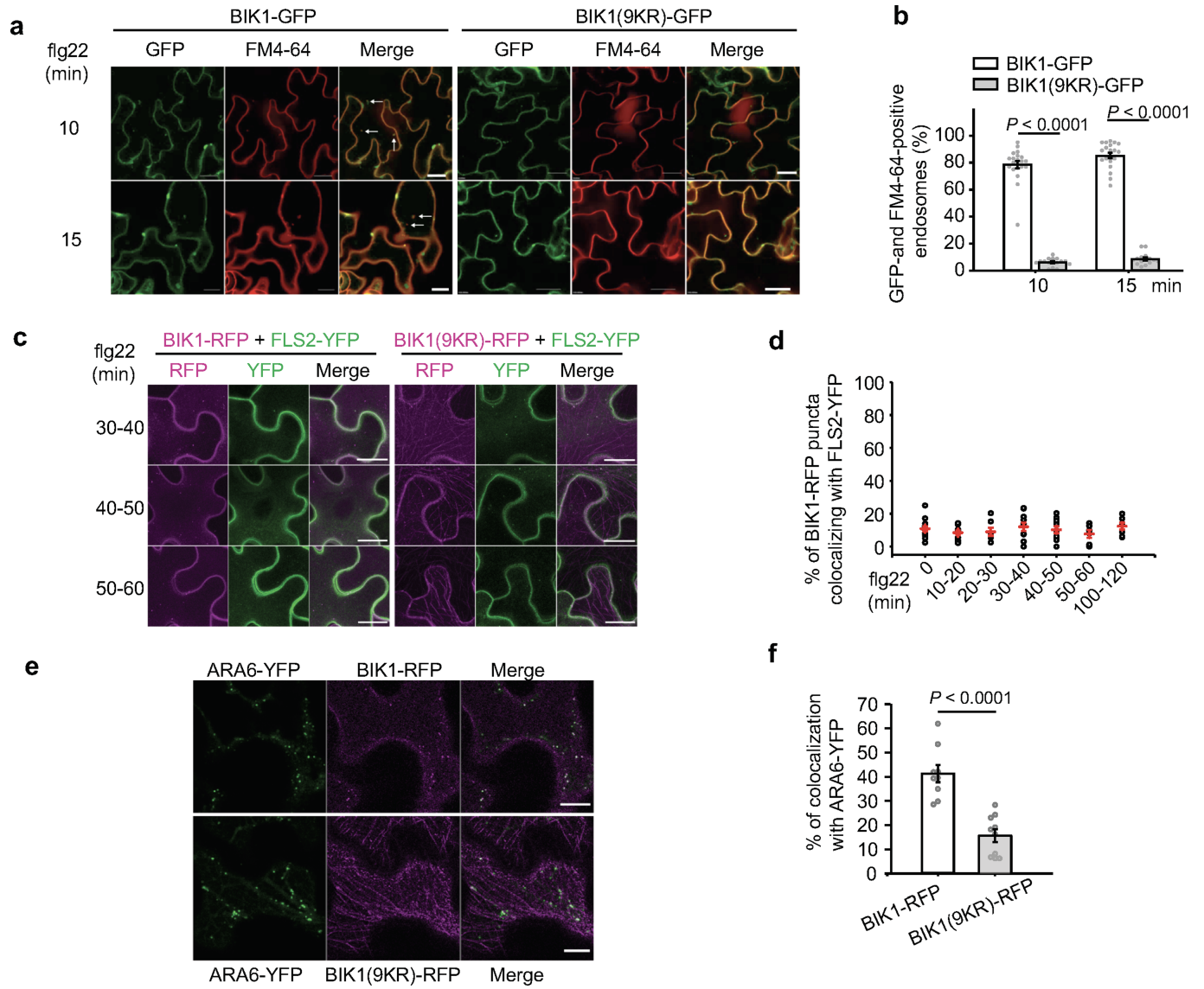

Extended Data Fig. 9 | The BIK1(9KR) mutation impairs flg22-induced endocytosis of BIK1. a, **b**, BIK1(9KR)–GFP puncta colocalize less than BIK1–GFP with FM4-64 upon treatment with flg22. **a**, Five-day-old *35S::BIK1-GFP* or *35S::BIK1^{9KR}-GFP* seedlings were pretreated with FM4-64 (2 μM) for 15 min and elicited with 100 nM flg22 for the indicated times; fluorescence was detected in epidermis using confocal microscopy. White arrows, colocalized endosomes. Scale bars, 20 μm. **b**, Percentage of endosomes positive for BIK1–GFP or BIK1(9KR)–GFP and FM4-64 over time per 100% of image area. Mean ± s.e.m. overlaid with dot plots (two-tailed Student's *t*-test, $n = 21$ images for BIK1–GFP and $n = 16, 15$ images for 10, 15 min, respectively, for BIK1(9KR)–GFP). **c**, Flg22-induced endocytosis of BIK1, BIK1(9KR) and FLS2 in *N. benthamiana*. BIK1–TagRFP (BIK1–RFP) or BIK1(9KR)–TagRFP (BIK1(9KR)–RFP) was co-expressed with FLS2–YFP in *N. benthamiana*, infiltrated with 100 μM flg22 and imaged at the indicated time points by confocal microscopy. Images at 30–40, 40–50 and 50–60 min after flg22 treatment from Fig. 4e are shown here. Scale bars, 20 μm. For BIK1–RFP/FLS2–YFP, $n = 14, 11, 7, 10, 10, 6, 7$ images for 0, 10–20, 20–30, 30–40, 40–50, 50–60, 100–120 min; for BIK1(9KR)–RFP/FLS2–YFP, $n = 19, 11, 11, 9, 16, 12, 7$ images for 0, 10–20, 20–30, 30–40, 40–50, 50–60, 100–120 min, respectively. **d**, Percentage of BIK1–RFP puncta that colocalized with FLS2–YFP after treatment with flg22 for the indicated times in **c** and Fig. 4e. Mean ± s.e.m. overlaid with dot plots ($n = 14, 11, 7, 10, 10, 6, 7$ images for 0, 10–20, 20–30, 30–40, 40–50, 50–60, 100–120 min, respectively). **e**, **f**, BIK1(9KR)–RFP shows reduced colocalization with ARA6–YFP. **e**, BIK1–RFP or BIK1(9KR)–RFP was transiently expressed with ARA6–YFP in *N. benthamiana*, and the images were taken 48–72 h after infiltration. Scale bars, 10 μm. **f**, Percentage of BIK1–RFP puncta that colocalized with ARA6–YFP. Mean ± s.e.m. overlaid with dot plots (two-tailed Student's *t*-test, $n = 9$ images for BIK1–RFP; $n = 10$ images for BIK1(9KR)–RFP). Experiments were repeated three times with similar results.

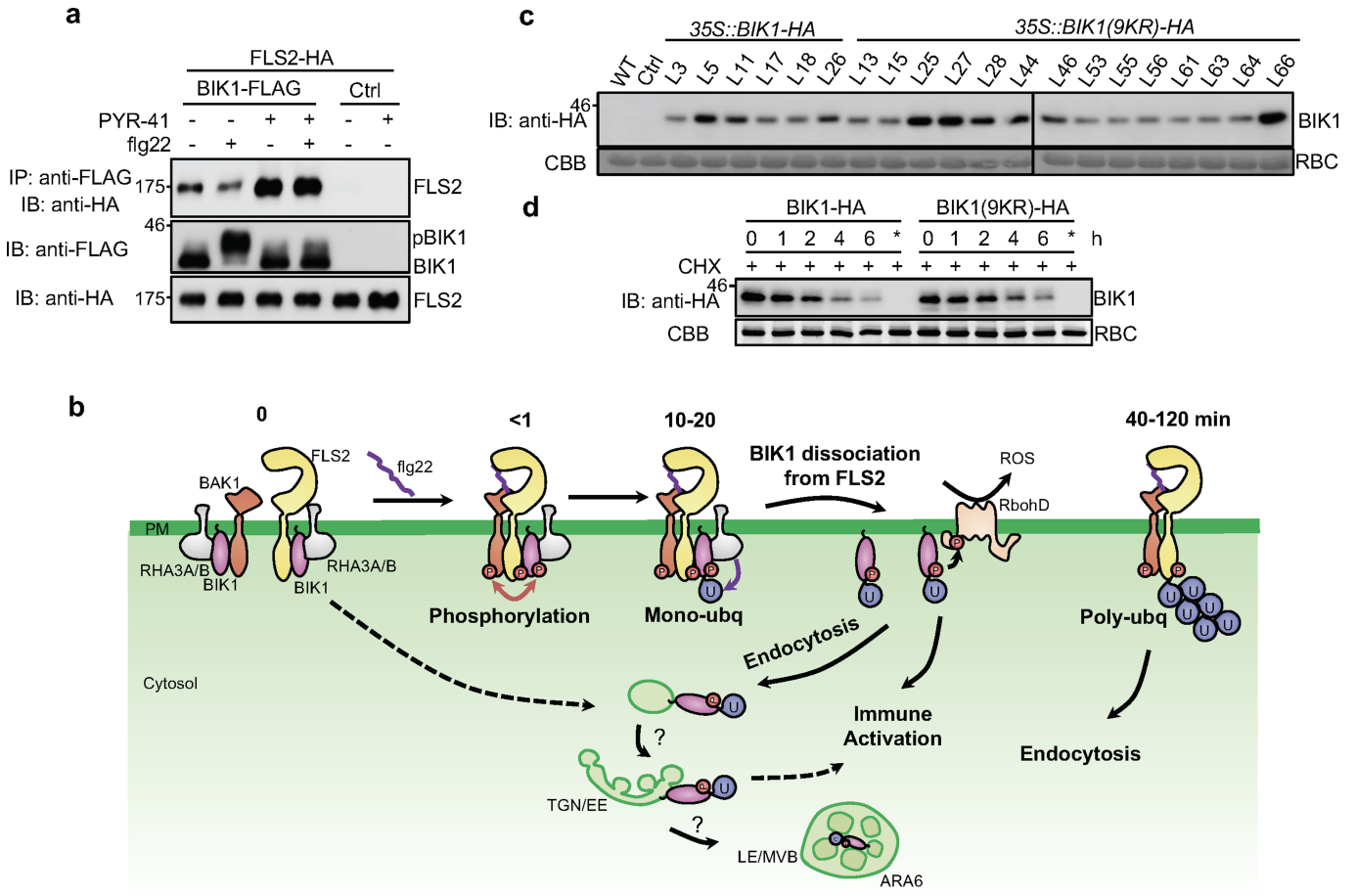

Extended Data Fig. 10 | Monoubiquitination mediates release of BIK1 from the plasma membrane upon ligand detection. a, PYR-41 impairs flg22-induced dissociation of BIK1 from FLS2. FLS2–HA was co-expressed with BIK1–FLAG or control in protoplasts. After pretreatment with 50 μM PYR-41 for 30 min, protoplasts were stimulated with 100 nM flg22 for 15 min. Co-IP and immunoblotting were performed as in Fig. 4g. **b**, A working model of RHA3A/B-mediated BIK1 monoubiquitination in plant immunity. Under non-activated, steady-state conditions (0 min), BIK1 remains hypo-phosphorylated and associates with FLS2 and BAK1. Upon flg22 detection, FLS2 dimerizes with BAK1, which stimulates BIK1 phosphorylation (<1 min). Phosphorylated BIK1 is monoubiquitinated by the E3 ligases RHA3A and RHA3B, leading to dissociation of BIK1 from the FLS2–BAK1 complex, accompanied by endocytosis (10–20 min). Ligand-induced monoubiquitination of BIK1 contributes to the activation of ROS and other defence responses. FLS2 is polyubiquitinated and endocytosed 40 min after detection of flg22 to attenuate signalling. **c**, BIK1(9KR) shows comparable protein expression to BIK1 in transgenic plants. *35S::BIK1-HA* or *35S::BIK1^{9KR}-HA* transgenic plants in wild-type background were used for immunoblotting to detect BIK1 proteins with anti-HA antibody. Control, empty vector. **d**, Stability of BIK1 and BIK1(9KR) proteins after treatment with cycloheximide (CHX). BIK1–HA or BIK1(9KR)–HA was expressed in wild-type protoplasts for 12 h followed by treatment with 500 μg/ml CHX for the indicated time. BIK1 or BIK1(9KR) proteins were analysed by immunoblotting with anti-HA antibody. Asterisk indicates that CHX was added immediately after transfection, thus blocking protein synthesis. Experiments were repeated three times with similar results.

nature research

Corresponding author(s): Libo Shan

Reporting Summary

Nature Research wishes to improve the reproducibility of the work that we publish. This form provides structure for consistency and transparency in reporting. For further information on Nature Research policies, see Authors & Referees and the Editorial Policy Checklist.

Statistical parameters

When statistical analyses are reported, confirm that the following items are present in the relevant location (e.g. figure legend, table legend, main text, or Methods section).

n/a	Confirmed	
☐	☒	The exact sample size (*n*) for each experimental group/condition, given as a discrete number and unit of measurement
☐	☒	An indication of whether measurements were taken from distinct samples or whether the same sample was measured repeatedly
☐	☒	The statistical test(s) used AND whether they are one- or two-sided *Only common tests should be described solely by name; describe more complex techniques in the Methods section.*
☐	☒	A description of all covariates tested
☐	☒	A description of any assumptions or corrections, such as tests of normality and adjustment for multiple comparisons
☐	☒	A full description of the statistics including central tendency (e.g. means) or other basic estimates (e.g. regression coefficient) AND variation (e.g. standard deviation) or associated estimates of uncertainty (e.g. confidence intervals)
☐	☒	For null hypothesis testing, the test statistic (e.g. *F*, *t*, *r*) with confidence intervals, effect sizes, degrees of freedom and *P* value noted *Give P values as exact values whenever suitable.*
☒	☐	For Bayesian analysis, information on the choice of priors and Markov chain Monte Carlo settings
☒	☐	For hierarchical and complex designs, identification of the appropriate level for tests and full reporting of outcomes
☒	☐	Estimates of effect sizes (e.g. Cohen's *d*, Pearson's *r*), indicating how they were calculated
☐	☒	Clearly defined error bars *State explicitly what error bars represent (e.g. SD, SE, CI)*

Our web collection on statistics for biologists may be useful.

Software and code

Policy information about availability of computer code

Data collection	Image J (version 1.51), Image Lab (Bio-Rad, version 4.1), LAS-X (Leica, version 3.5.6.21594) were used in data collection.
Data analysis	Images from Immuno Blotting were quantified with Image LabTM (Bio-Rad, version 4.1). Confocal images were analyzed with LAS-X (Leica, version 3.5.6.21594), ZEN (Zeiss). Statistical analysis was performed with Microsoft Excel 2016. The MS/MS spectra were analyzed with SEQUEST (version 28). Crystal structure was analyzed with PyMOL (version 2.1).

For manuscripts utilizing custom algorithms or software that are central to the research but not yet described in published literature, software must be made available to editors/reviewers upon request. We strongly encourage code deposition in a community repository (e.g. GitHub). See the Nature Research guidelines for submitting code & software for further information.

Data

Policy information about availability of data

All manuscripts must include a data availability statement. This statement should provide the following information, where applicable:

- Accession codes, unique identifiers, or web links for publicly available datasets
- A list of figures that have associated raw data
- A description of any restrictions on data availability

The data supporting the findings of this study are available within the paper and its Supplementary Information files. Source Data (gels and graphs) for Figs. 1–4 and Extended Data Figs. 1–10 are provided with the paper.

Field-specific reporting

Please select the best fit for your research. If you are not sure, read the appropriate sections before making your selection.

☒ Life sciences ☐ Behavioural & social sciences ☐ Ecological, evolutionary & environmental sciences

For a reference copy of the document with all sections, see nature.com/authors/policies/ReportingSummary-flat.pdf

Life sciences study design

All studies must disclose on these points even when the disclosure is negative.

Sample size	No statistical methods were used to predetermine sample sizes. Sample sizes were determined based on previous publications on similar experiments. The sample sizes were sufficient as the differences between experimental groups were reproducible.
Data exclusions	No data were excluded from analyses in the experiments.
Replication	All attempts to replicate the experiments were successful. Number of repeats was given in the figure legends.
Randomization	Plant materials used in the study were collected randomly.
Blinding	Investigators were not blinded to plant genotypes during experiments. The research materials are plants so the blinding design is not applicable to this system. Experiment results are not subjective.

Behavioural & social sciences study design

All studies must disclose on these points even when the disclosure is negative.

Study description	*Briefly describe the study type including whether data are quantitative, qualitative, or mixed-methods (e.g. qualitative cross-sectional, quantitative experimental, mixed-methods case study).*
Research sample	*State the research sample (e.g. Harvard university undergraduates, villagers in rural India) and provide relevant demographic information (e.g. age, sex) and indicate whether the sample is representative. Provide a rationale for the study sample chosen. For studies involving existing datasets, please describe the dataset and source.*
Sampling strategy	*Describe the sampling procedure (e.g. random, snowball, stratified, convenience). Describe the statistical methods that were used to predetermine sample size OR if no sample-size calculation was performed, describe how sample sizes were chosen and provide a rationale for why these sample sizes are sufficient. For qualitative data, please indicate whether data saturation was considered, and what criteria were used to decide that no further sampling was needed.*
Data collection	*Provide details about the data collection procedure, including the instruments or devices used to record the data (e.g. pen and paper, computer, eye tracker, video or audio equipment) whether anyone was present besides the participant(s) and the researcher, and whether the researcher was blind to experimental condition and/or the study hypothesis during data collection.*
Timing	*Indicate the start and stop dates of data collection. If there is a gap between collection periods, state the dates for each sample cohort.*
Data exclusions	*If no data were excluded from the analyses, state so OR if data were excluded, provide the exact number of exclusions and the rationale behind them, indicating whether exclusion criteria were pre-established.*
Non-participation	*State how many participants dropped out/declined participation and the reason(s) given OR provide response rate OR state that no participants dropped out/declined participation.*
Randomization	*If participants were not allocated into experimental groups, state so OR describe how participants were allocated to groups, and if allocation was not random, describe how covariates were controlled.*

Ecological, evolutionary & environmental sciences study design

All studies must disclose on these points even when the disclosure is negative.

Study description	*Briefly describe the study. For quantitative data include treatment factors and interactions, design structure (e.g. factorial, nested, hierarchical), nature and number of experimental units and replicates.*
Research sample	*Describe the research sample (e.g. a group of tagged Passer domesticus, all Stenocereus thurberi within Organ Pipe Cactus National Monument), and provide a rationale for the sample choice. When relevant, describe the organism taxa, source, sex, age range and any manipulations. State what population the sample is meant to represent when applicable. For studies involving existing datasets, describe the data and its source.*
Sampling strategy	*Note the sampling procedure. Describe the statistical methods that were used to predetermine sample size OR if no sample-size calculation was performed, describe how sample sizes were chosen and provide a rationale for why these sample sizes are sufficient.*
Data collection	*Describe the data collection procedure, including who recorded the data and how.*
Timing and spatial scale	*Indicate the start and stop dates of data collection, noting the frequency and periodicity of sampling and providing a rationale for these choices. If there is a gap between collection periods, state the dates for each sample cohort. Specify the spatial scale from which the data are taken*
Data exclusions	*If no data were excluded from the analyses, state so OR if data were excluded, describe the exclusions and the rationale behind them, indicating whether exclusion criteria were pre-established.*
Reproducibility	*Describe the measures taken to verify the reproducibility of experimental findings. For each experiment, note whether any attempts to repeat the experiment failed OR state that all attempts to repeat the experiment were successful.*
Randomization	*Describe how samples/organisms/participants were allocated into groups. If allocation was not random, describe how covariates were controlled. If this is not relevant to your study, explain why.*
Blinding	*Describe the extent of blinding used during data acquisition and analysis. If blinding was not possible, describe why OR explain why blinding was not relevant to your study.*

Did the study involve field work? ☐ Yes ☐ No

Field work, collection and transport

Field conditions	*Describe the study conditions for field work, providing relevant parameters (e.g. temperature, rainfall).*
Location	*State the location of the sampling or experiment, providing relevant parameters (e.g. latitude and longitude, elevation, water depth).*
Access and import/export	*Describe the efforts you have made to access habitats and to collect and import/export your samples in a responsible manner and in compliance with local, national and international laws, noting any permits that were obtained (give the name of the issuing authority, the date of issue, and any identifying information).*
Disturbance	*Describe any disturbance caused by the study and how it was minimized.*

Reporting for specific materials, systems and methods

Materials & experimental systems

n/a	Involved in the study
☒	☐ Unique biological materials
☐	☒ Antibodies
☒	☐ Eukaryotic cell lines
☒	☐ Palaeontology
☒	☐ Animals and other organisms
☒	☐ Human research participants

Methods

n/a	Involved in the study
☒	☐ ChIP-seq
☒	☐ Flow cytometry
☒	☐ MRI-based neuroimaging

Unique biological materials

Policy information about availability of materials

Obtaining unique materials

Describe any restrictions on the availability of unique materials OR confirm that all unique materials used are readily available from the authors or from standard commercial sources (and specify these sources).

Antibodies

Antibodies used

Anti-HA-Peroxidase, Roche, Cat # 12013819001, clone 3F10. Dilution 1: 2,000.
Anti-FLAG-Peroxidase, Sigma-Aldrich, Cat # A8592, clone M2. Dilution 1: 2,000.
Anti-GST, Santa Cruz, Cat # SC-53909, clone 1E5. Dilution 1: 2,000.
Anti-ubiquitin (P4D1), Santa Cruz, Cat # SC-8017, clone P4D1. Dilution 1:500.
Anti-GFP, Roche, Cat # 11814460001, mix of clone 7.1 and 13.1. Dilution 1: 2,000.
Anti-Phospho-p44/42 MAPK, Cell Signaling, Cat # 9101. Polyclone. Dilution 1: 2,000.
Anti-Rabbit IgG, HRP-linked antibody, Cell Signaling, Cat # 7074. Polyclone. Dilution 1: 10,000.
Anti-Mouse IgG, HRP-linked antibody, Cell Signaling, Cat # 7076. Polyclone. Dilution 1: 10,000.
Anti-FLAG M2 Affinity gel, Sigma-Aldrich, Cat # 2220, clone M2.
Anti-MBP, Biolegend, Cat # 906901, clone YM-2. Dilution 1: 1,000.
Anti-RHA3A, GenScript, generated with peptide AGGDSPSPNKGLKKC. Polyclone. Dilution 1:1,000.

Validation

Validation statements, relevant citations of commercial primary antibodies are available from manufacturers:
Anti-HA-Peroxidase, Roche, Cat # 12013819001, clone 3F10. https://www.sigmaaldrich.com/catalog/product/roche/12013819001?lang=en&region=US
Anti-FLAG-Peroxidase, Sigma-Aldrich, Cat # A8592, clone M2. https://www.sigmaaldrich.com/catalog/product/sigma/a8592?lang=en&region=US
Anti-GST, Santa Cruz, Cat # SC-53909, clone 1E5. https://www.scbt.com/p/gst-antibody-1e5
Anti-ubiquitin (P4D1), Santa Cruz, Cat # SC-8017, clone P4D1. https://www.scbt.com/p/ub-antibody-p4d1
Anti-GFP, Roche, Cat # 11814460001, mix of clone 7.1 and 13.1. https://www.sigmaaldrich.com/catalog/product/roche/11814460001?lang=en&region=US
Anti-Phospho-p44/42 MAPK, Cell Signaling, Cat # 9101. https://www.cellsignal.com/products/primary-antibodies/phospho-p44-42-mapk-erk1-2-thr202-tyr204-antibody/9101
Anti-Rabbit IgG, HRP-linked antibody, Cell Signaling, Cat # 7074. https://www.cellsignal.com/products/secondary-antibodies/anti-rabbit-igg-hrp-linked-antibody/7074
Anti-Mouse IgG, HRP-linked antibody, Cell Signaling, Cat # 7076. https://www.cellsignal.com/products/secondary-antibodies/anti-mouse-igg-hrp-linked-antibody/7076
Anti-FLAG M2 Affinity gel, Sigma-Aldrich, Cat # 2220, clone M2. https://www.sigmaaldrich.com/catalog/product/sigma/a2220?lang=en&region=US
Anti-MBP, Biolegend, Cat # 906901, clone YM-2. https://www.biolegend.com/en-gb/products/purified-anti-maltose-binding-protein-mbp-antibody-11081
Anti-RHA3A, GenScript, generated with peptide AGGDSPSPNKGLKKC from Rabbit. Figure 2d bottom panel supports the anti-RHA3A antibody do not have cross reactivity with other protein including E1, E2, BIK1 or Ubiquitin.

Eukaryotic cell lines

Policy information about cell lines

Cell line source(s)

State the source of each cell line used.

Authentication

Describe the authentication procedures for each cell line used OR declare that none of the cell lines used were authenticated.

Mycoplasma contamination

Confirm that all cell lines tested negative for mycoplasma contamination OR describe the results of the testing for mycoplasma contamination OR declare that the cell lines were not tested for mycoplasma contamination.

Commonly misidentified lines
(See ICLAC register)

No commonly misidentified cell lines were used.

Palaeontology

Specimen provenance

Provide provenance information for specimens and describe permits that were obtained for the work (including the name of the issuing authority, the date of issue, and any identifying information).

Specimen deposition

Indicate where the specimens have been deposited to permit free access by other researchers.

Dating methods	*If new dates are provided, describe how they were obtained (e.g. collection, storage, sample pretreatment and measurement), where they were obtained (i.e. lab name), the calibration program and the protocol for quality assurance OR state that no new dates are provided.*

☐ Tick this box to confirm that the raw and calibrated dates are available in the paper or in Supplementary Information.

Animals and other organisms

Policy information about studies involving animals; ARRIVE guidelines recommended for reporting animal research

Laboratory animals	*For laboratory animals, report species, strain, sex and age OR state that the study did not involve laboratory animals.*
Wild animals	*Provide details on animals observed in or captured in the field; report species, sex and age where possible. Describe how animals were caught and transported and what happened to captive animals after the study (if killed, explain why and describe method; if released, say where and when) OR state that the study did not involve wild animals.*
Field-collected samples	*For laboratory work with field-collected samples, describe all relevant parameters such as housing, maintenance, temperature, photoperiod and end-of-experiment protocol OR state that the study did not involve samples collected from the field.*

Human research participants

Policy information about studies involving human research participants

Population characteristics	*Describe the covariate-relevant population characteristics of the human research participants (e.g. age, gender, genotypic information, past and current diagnosis and treatment categories). If you filled out the behavioural & social sciences study design questions and have nothing to add here, write "See above."*
Recruitment	*Describe how participants were recruited. Outline any potential self-selection bias or other biases that may be present and how these are likely to impact results.*

ChIP-seq

Data deposition

☐ Confirm that both raw and final processed data have been deposited in a public database such as GEO.

☐ Confirm that you have deposited or provided access to graph files (e.g. BED files) for the called peaks.

Data access links *May remain private before publication.*	*For "Initial submission" or "Revised version" documents, provide reviewer access links. For your "Final submission" document, provide a link to the deposited data.*
Files in database submission	*Provide a list of all files available in the database submission.*
Genome browser session (e.g. UCSC)	*Provide a link to an anonymized genome browser session for "Initial submission" and "Revised version" documents only, to enable peer review. Write "no longer applicable" for "Final submission" documents.*

Methodology

Replicates	*Describe the experimental replicates, specifying number, type and replicate agreement.*
Sequencing depth	*Describe the sequencing depth for each experiment, providing the total number of reads, uniquely mapped reads, length of reads and whether they were paired- or single-end.*
Antibodies	*Describe the antibodies used for the ChIP-seq experiments; as applicable, provide supplier name, catalog number, clone name, and lot number.*
Peak calling parameters	*Specify the command line program and parameters used for read mapping and peak calling, including the ChIP, control and index files used.*
Data quality	*Describe the methods used to ensure data quality in full detail, including how many peaks are at FDR 5% and above 5-fold enrichment.*
Software	*Describe the software used to collect and analyze the ChIP-seq data. For custom code that has been deposited into a community repository, provide accession details.*

Flow Cytometry

Plots

Confirm that:

☐ The axis labels state the marker and fluorochrome used (e.g. CD4-FITC).

☐ The axis scales are clearly visible. Include numbers along axes only for bottom left plot of group (a 'group' is an analysis of identical markers).

☐ All plots are contour plots with outliers or pseudocolor plots.

☐ A numerical value for number of cells or percentage (with statistics) is provided.

Methodology

Sample preparation	*Describe the sample preparation, detailing the biological source of the cells and any tissue processing steps used.*
Instrument	*Identify the instrument used for data collection, specifying make and model number.*
Software	*Describe the software used to collect and analyze the flow cytometry data. For custom code that has been deposited into a community repository, provide accession details.*
Cell population abundance	*Describe the abundance of the relevant cell populations within post-sort fractions, providing details on the purity of the samples and how it was determined.*
Gating strategy	*Describe the gating strategy used for all relevant experiments, specifying the preliminary FSC/SSC gates of the starting cell population, indicating where boundaries between "positive" and "negative" staining cell populations are defined.*

☐ Tick this box to confirm that a figure exemplifying the gating strategy is provided in the Supplementary Information.

Magnetic resonance imaging

Experimental design

Design type	*Indicate task or resting state; event-related or block design.*
Design specifications	*Specify the number of blocks, trials or experimental units per session and/or subject, and specify the length of each trial or block (if trials are blocked) and interval between trials.*
Behavioral performance measures	*State number and/or type of variables recorded (e.g. correct button press, response time) and what statistics were used to establish that the subjects were performing the task as expected (e.g. mean, range, and/or standard deviation across subjects).*

Acquisition

Imaging type(s)	*Specify: functional, structural, diffusion, perfusion.*
Field strength	*Specify in Tesla*
Sequence & imaging parameters	*Specify the pulse sequence type (gradient echo, spin echo, etc.), imaging type (EPI, spiral, etc.), field of view, matrix size, slice thickness, orientation and TE/TR/flip angle.*
Area of acquisition	*State whether a whole brain scan was used OR define the area of acquisition, describing how the region was determined.*

Diffusion MRI ☐ Used ☐ Not used

Preprocessing

Preprocessing software	*Provide detail on software version and revision number and on specific parameters (model/functions, brain extraction, segmentation, smoothing kernel size, etc.).*
Normalization	*If data were normalized/standardized, describe the approach(es): specify linear or non-linear and define image types used for transformation OR indicate that data were not normalized and explain rationale for lack of normalization.*
Normalization template	*Describe the template used for normalization/transformation, specifying subject space or group standardized space (e.g. original Talairach, MNI305, ICBM152) OR indicate that the data were not normalized.*
Noise and artifact removal	*Describe your procedure(s) for artifact and structured noise removal, specifying motion parameters, tissue signals and physiological signals (heart rate, respiration).*
Volume censoring	*Define your software and/or method and criteria for volume censoring, and state the extent of such censoring.*

Statistical modeling & inference

Model type and settings

Specify type (mass univariate, multivariate, RSA, predictive, etc.) and describe essential details of the model at the first and second levels (e.g. fixed, random or mixed effects; drift or auto-correlation).

Effect(s) tested

Define precise effect in terms of the task or stimulus conditions instead of psychological concepts and indicate whether ANOVA or factorial designs were used.

Specify type of analysis: ☐ Whole brain ☐ ROI-based ☐ Both

Statistic type for inference
(See Eklund et al. 2016)

Specify voxel-wise or cluster-wise and report all relevant parameters for cluster-wise methods.

Correction

Describe the type of correction and how it is obtained for multiple comparisons (e.g. FWE, FDR, permutation or Monte Carlo).

Models & analysis

n/a	Involved in the study
☐	☐ Functional and/or effective connectivity
☐	☐ Graph analysis
☐	☐ Multivariate modeling or predictive analysis

Functional and/or effective connectivity

Report the measures of dependence used and the model details (e.g. Pearson correlation, partial correlation, mutual information).

Graph analysis

Report the dependent variable and connectivity measure, specifying weighted graph or binarized graph, subject- or group-level, and the global and/or node summaries used (e.g. clustering coefficient, efficiency, etc.).

Multivariate modeling and predictive analysis

Specify independent variables, features extraction and dimension reduction, model, training and evaluation metrics.